Chapter 5: Global Carbon and other Biogeochemical Cycles and Feedbacks – Supplementary Material

Coordinating Lead Authors:
Josep G. Canadell (Australia), Pedro M.S. Monteiro (South Africa)

Lead Authors:
Marcos H. Costa (Brazil), Leticia Cotrim da Cunha (Brazil), Peter Cox (UK), Alexey V. Eliseev (Russia), Stephanie Henson (UK), Masao Ishii (Japan), Samuel Jaccard (Switzerland), Charles Koven (USA), Annalea Lohila (Finland), Prabir Patra (Japan/India), Shilong Piao (China), Joeri, Rogelj (UK/Belgium), Stephen Syampungani (Zambia), Sönke Zaehle (Germany), Kirsten Zickfeld (Canada/Germany)

Contributing Authors:
Georgii A. Alexandrov (Russia), Govindasamy Bala (India/USA), Laurent Bopp (France), Lena Boysen (Germany), Long Cao (China), Naveen Chandra (Japan/India), Philippe Ciais (France), Sergey N. Denisov (Russia), Frank Dentener (EU, Netherlands), Hervé Douville (France), Amanda Fay (USA), Piers Forster (UK), Baylor Fox-Kemper (USA), Pierre Friedlingstein (UK), Weiwei Fu (China/USA), Sabine Fuss (Germany), Véronique Garçon (France), Bettina Gier (Germany), Nathan Gillett (Canada), Luke Gregor (Switzerland/South Africa), Karsten Haustein (Germany), Vanessa Haverd (Australia), Jian He (U.S.A/P.R. China), Forrest Hoffman (USA), Tatiana Ilyina (Germany), Robert Jackson (USA), Chris Jones (UK), David Keller (USA/Germany), Lester Kwiatkowski (France/UK), Robin D. Lamboll (UK/USA,UK), Xin Lan (U.S.A/P.R.China), Charlotte Laufkötter (Switzerland/Germany), Corinne Le Quéré (UK), Andrew Lenton (Australia), Jared Lewis (Australia/New Zealand), Spencer Liddicoat (UK), Laura Lorenzoni (USA/Venezuela), Nicole Lovenduski (USA), Andrew MacDougall (Canada), Sabine Mathesius (Canada/Germany), Damon Matthews (Canada), Malte Meinshausen (Australia/Germany), Igor I. Mokhov (Russia), Vaishali Naik (USA), Zebedee Nicholls (Australia), Intan Suci Nurhati (Indonesia), Michael O'Sullivan (UK), Glen Peters (Norway), Julia Pongratz (Germany), Benjamin Poulter (USA), Jean-Baptiste Sallée (France/France), Edward A.G. Schuur (USA), Sonia I. Seneviratne (Switzerland), Ann Stavert (Australia), Parvadha Suntharalingam (UK/USA), Kaoru Tachiiri (Japan), Jens Terhaar (Switzerland/Germany), Rona Thompson (Norway, Luxembourg / New Zealand), Hanqin Tian (USA), Jocelyn Turnbull (New Zealand), Sergio M. Vicente-Serrano (Spain), Xuhui Wang (China), Rik Wanninkhof (USA), Phil Williamson (UK),

Review Editors:
Victor Brovkin (Germany/Russia), Richard Feely (USA)

Chapter Scientist:
Alice D. Lebehot (South Africa/France)

Date of Draft:
3/05/2021

Notes:
TSU compiled version

Table of Contents

5.SM.1 Assessment of recent advances in observational and modelling methodologies

Since AR5 three major advances have had a decisive impact on the levels of confidence of the trends and the variability of both air-sea fluxes of CO_2 and its storage in the ocean interior. These are (i) the new observations and observational-based products for decadal variability in ocean uptake fluxes and ocean storage, (ii) the observational-based product changes in amplitude of the seasonal cycle of surface ocean pCO_2 (the partial pressure of CO_2 expressed in μatm) in response to changing ocean carbonate chemistry, and (iii) spatially-resolved pCO_2 seasonal climatologies for the global coastal ocean (Gruber et al., 2019a; (Rödenbeck et al., 2015; Landschützer et al., 2016, 2018); Laruelle et al., 2017). These advances were made possible by the simultaneous global coordination of observations and data quality control through the surface ocean CO_2 atlas (SOCAT) and Lamont-Doherty Earth observatory (LDEO) as well as the rapid adoption of a large variety of interpolation techniques for the surface layer and their inter-comparison to constrain uncertainties and biases (Rödenbeck et al., 2015; Bakker et al., 2016; Landschützer et al., 2016; McKinley et al., 2017; Gregor et al., 2019; Gruber et al., 2019b).

Advances in the multiple methods of interpolating surface ocean pCO_2 observations provide a *medium to high confidence* in the air-sea fluxes of CO_2 over most of the ocean (Rödenbeck et al., 2015; Landschützer et al., 2016; Gregor et al., 2019). However, there is *low confidence* in those fluxes for important regions such as the Southern Ocean, the Arctic, South Pacific as well as coastal oceans (Laruelle et al., 2017; Gregor et al., 2019; Gruber et al., 2019c); while these regions remain temporally and spatially under sampled the development and deployment of carbon and biogeochemically enabled Argo autonomous floats is starting to close those gaps (Williams et al., 2017; Gray et al., 2018; Claustre et al., 2020).

Similarly, for anthropogenic carbon storage in the ocean interior (i.e. below the mixed layer) the global ocean ship-based hydrographic investigations programme (GO-SHIP) coupled to the global ocean data analysis project for carbon (GLODAPv2) were central to supporting the advances in characterising changes to the storage in the ocean interior by generating a new consistent, quality-controlled, global dataset, allowing the decadal variability in ocean carbon storage to be quantified (Lauvset et al., 2016; Olsen et al., 2016; Clement and Gruber, 2018; Gruber et al., 2019b). There is *high confidence* that a significant advance since AR5 and SROCC is the improved characterization of the variability of the ocean CO_2 storage trends in space and time, which has notable decadal and regional scale variability (Tanhua et al., 2017; Gruber et al., 2019b) (SROCC Chapters 3 and 5).

Since it is also unequivocal that anthropogenic CO_2 taken up from the atmosphere into the ocean surface layer is further transported into the ocean interior through ocean ventilation processes including vertical mixing, diffusion, subduction and meridional overturning circulations (Sallée et al., 2012; Nakano et al., 2015; Bopp et al., 2015; Iudicone et al., 2016; Toyama et al., 2017), the trends as well as the spatial and temporal variability were assessed in an integrated way for both the air-sea flux and storage of anthropogenic CO_2.

5.SM.2 SeaFlux method: a 4 step methodological approach to address the first order inconsistencies between the ocean six (6) CO_2 flux observational based products used in Chapter 5 (5.2.3.1)

Contributors: Amanda Fay and Luke Gregor

Methods

The SeaFlux method is based on six published and widely used observation-based products of surface ocean partial pressure (of CO_2 (pCO_2) and spans years 1988–2018 (Gregor and Fay, 2021). These six include three neural network derived products (MPI-SOMFFN, CMEMS-FFNN, NIES-FNN), a mixed layer scheme product (JENA-MLS), a multiple linear regression (JMA-MLR), and a machine learning ensemble (CSIR-ML6) (Supplementary Materials Table 5.SM.1). These products are included as they have been regularly updated to extend their time period and incorporate additional data that comes with each annual release of the SOCAT database.

Surface pCO_2 observations play a key role in constraining the global ocean carbon sink. This is because variations in surface ocean pCO_2 is the driving force governing the exchange of CO_2 across the air-sea interface, which is commonly described through a bulk formula (Garbe et al., 2014; Wanninkhof, 2014):

$$\text{Flux} = k_w \cdot sol \cdot (pCO_2 - pCO_2^{atm}) \cdot (1 - ice) \quad (1)$$

where k_w is the gas transfer velocity, *sol* is the solubility of CO_2 in seawater, in units mol m^{-3} μatm^{-1}, pCO_2 is the partial pressure of surface ocean CO_2 in µatm, and pCO^{atm} in units of µatm represents the partial pressure of atmospheric CO_2 in the marine boundary layer. Finally, to account for the seasonal ice cover in high latitudes the fluxes are weighted by 1 minus the ice fraction (*ice*), *i.e.* the open ocean fraction.

All of these methods provide full three-dimensional fields (latitude, longitude, time) of the sea surface partial pressure of CO_2 (pCO_2) and the air-sea CO_2 flux. In their original form each product may utilise different choices for the inputs to Equation 1. In this work recompute the fluxes using the following inputs to the bulk parameterization approach Equation 1: k_w is the gas transfer velocity, *sol* is the solubility of CO_2 in seawater, in units mol m^{-3} μatm^{-1}, calculated using the formulation by Weiss, (1974), EN4 salinity (Good et al., 2013), Operational Sea Surface Temperature and Sea Ice Analysis (OSTIA) sea surface temperature (Good et al., 2020), and European Centre for Medium- Range Weather Forecasts (ECMWF) ERA5 sea level pressure (Hersbach et al., 2020); *ice* is the sea ice fraction from OSTIA (Good et al., 2020); pCO_2 is the partial pressure of oceanic CO_2 in µatm for each observation-based product after filling, and pCO_2^{atm} is the dry air mixing ratio of atmospheric CO_2 (xCO_2) from the ESRL surface marine boundary layer CO_2 product available at https://www.esrl.noaa.gov/gmd/ccgg/mbl/data.php (Dlugokencky and Tans, 2020) multiplied by ERA5 sea level pressure (Hersbach et al., 2020) at monthly resolution, and applying the water vapor correction according to Dickson et al. (2007).

Flux is defined positive upward, that is CO_2 release from the ocean into the atmosphere is positive, and uptake by the ocean is negative. In the following sections we discuss the three steps that have the greatest impact on the inconsistencies between unadjusted flux calculations in the six pCO_2 products and the approach that we utilise for the SeaFlux ensemble product.

Step 1: Area filling

Machine learning methods aim to maximise the utility of the existing in situ observations by extrapolation using various proxy variables for processes influencing changes in ocean pCO_2. Extrapolation with these independently observed variables is possible due to the nonlinear relationship between pCO_2 in the surface ocean and the proxies that drive these changes.

However, not all of the proxy variables have complete global ocean coverage for all months, so the resulting pCO_2 products are limited by the extent of the proxy variables. Additionally, in coastal regions there is the potential that different relationships of pCO_2 are expected than in the open ocean, thus limiting the extrapolations. In contrast, the mixed layer scheme (utilised by the JENA-MLS product) does not suffer from such missing areas but does not distinguish between coastal and open ocean. While the area extent of the available air-sea flux estimates varies between products, there are consistent patterns; nearly all products cover the open ocean, whereas larger differences exist in the coverage of coastal regions, shelf seas, marginal seas and the Arctic Ocean. To account for differing area coverage, past studies (Friedlingstein et al., 2019, 2020; Hauck et al., 2020) have adjusted simply by scaling based on the percent of the total ocean area covered by each observation-based product. This does not account for the fact that some areas have CO_2 flux densities that are higher or lower than the global average. Thus, the magnitude of the adjustment by area-scaling is likely an underestimate (McKinley et al., 2020). One specific example is the northern high latitudes where coverage by the six products varies substantially. Similarly, three products provide estimates in marginal seas such as the Mediterranean while the other three products have no reported pCO_2 values here. Shutler et al., (2016) report that subtle differences in regional definitions can cause differences of >10% in the calculated net fluxes.

To address the inconsistent spatial coverage in products we utilise a newly released open and coastal merged climatology product (MPI-ULB-SOMFFN; Landschützer et al., 2020b) that is a blend of the coastal ocean SOMFFN mapping method (Laruelle et al., 2017) and the open ocean equivalent (MPI-SOMFFN; Landschützer et al., 2020a), but which now includes missing coastal ocean regions, marginal seas and the full Arctic Ocean. For each observationally-based product, we fill missing grid cells with a scaled value based on this global-coverage climatology. The scaling accounts for year-to- year changes in pCO_2 in the missing areas (given that the extended MPI-ULB-SOMFFN product is a monthly climatology centred on year 2006) and is obtained as follows. To extend the open and coastal merged monthly climatology (MPI-ULB-SOMFFN) to 1988–2018, we calculate a global scaling factor based on the product-based ensemble mean pCO_2 for regions which are covered consistently by all six pCO_2 products. We first mask all pCO_2 products to a common sea mask before taking an ensemble mean (pCO_2^{ens}). Next, we divide this ensemble mean by the MPI-ULB-SOMFFN climatology (pCO_2^{clim}) at monthly 1° by 1° resolution (Equation 2). The monthly scaling factor ($sf\,pCO_2$) is calculated by taking the mean over the spatial dimensions.

The scaling factor calculation can be represented as:

$$sf_{pCO_2} = mean_{x,y}\left(\frac{pCO_2^{ens}}{pCO_2^{clim}}\right) \qquad (2)$$

where $sf pCO_2$ is the one-dimensional scaling factor (time dimension), pCO_2^{ens} is the ensemble mean of all pCO_2 products at three-dimension, monthly 1° by 1° resolution, pCO_2^{clim} is the MPI-ULB-SOMFFN climatology, also at three-dimension but limited to just one climatological year. The *x* and *y* indicate that we take the area-weighted average over longitude (*x*) and latitude (*y*) resulting in the monthly scaling value. If a product mean is exactly equal to the climatology mean, the scaling factor is 1. Value ranges from 0.91 to 1.06 over the 31-year time period. The one-dimensional scaling factor is then multiplied by the MPI-ULB-SOMFFN climatology for each spatial point resulting in a three-dimensional scaled filling map. These values are then used to fill in missing grid cells in each observation-based product. Globally, the adjustments are all less than 20% of the total flux, with the mean adjustment for the six products at 9%. In the Northern Hemisphere however, the filling process can drive adjustments of up to 35%. As expected, the observationally-based products with more complete spatial coverage tend to have smaller flux adjustments, however the impact on the final CO_2 flux depends on the ΔpCO_2 and wind speed of the areas being filled. The only product that does not change during this adjustment process is the JENA-MLS mixed layer scheme-based product (Rödenbeck et al., 2013) which is produced with full spatial coverage and therefore needs no spatial filling.

Our approach is not without its own assumptions and limitations. We rely on a single estimate of the missing pCO_2 in coastal ocean regions, marginal seas, and the full Arctic Ocean, given that this is the only publicly available product currently existing. Nevertheless, the fact that common missing areas along coastal regions and marginal seas are reconstructed using specific coastal observations provides a step forward from the linear-scaling approach currently used by the Global Carbon Budget (Friedlingstein et al., 2019, 2020). Further confidence is provided by previous research showing that climatological relevant signals, i.e. mean state and seasonality, are well reconstructed by the MPI-SOMFFN method.

Furthermore, our scaled filling methodology assumes that pCO_2 in the missing ocean regions is increasing at the same rate as the common area of open-ocean pCO_2 used to calculate the scaling factor. Research from coastal ocean regions and shelf seas reveal that, in spite of a large spatial heterogeneity, this is a reasonable first order approximation (Laruelle et al., 2017). While our approach has a constant scaling factor for the missing ocean areas regardless of latitude we acknowledge that this could be improved with increased understanding.

Step 2: Wind product selection

180 Historical wind speed observations (including measurements from satellites and moored buoys) are aggregated and extrapolated through modelling and data assimilation systems to create global wind reanalyses. These reanalyses are required to compute air-sea gas exchange. Air-sea flux is commonly parameterised as a function of the gradient of CO_2 between the ocean and the atmosphere with wind speed

modulating the rate of the gas exchange (Equation 1). Each of these wind reanalyses has strengths and weaknesses, specifically on regional and seasonal scales (Chaudhuri et al., 2014; Ramon et al., 2019) but all are considered reasonable options by the community (Roobaert et al., 2018). We use three wind reanalysis products for completeness: the Cross-Calibrated Multi-Platform v2 (CCMP2, (Atlas et al., 2011)), the Japanese 55-year Reanalysis (JRA-55, KOBAYASHI et al., 2015) and the European Centre for Medium-Range Weather Forecasts (ECMWF) ERA5 (Hersbach et al., 2020). The wind speed (U10) is calculated at the native resolution of each wind product from the u- and v-components of wind.

Step 3: Calculation of gas exchange coefficient

We employ the quadratic windspeed dependence of the gas transfer velocity (Wanninkhof, 1992) and calculate the piston velocity (*kw*) for each of the wind reanalysis products as:

$$k_W = a \cdot \langle U^2 \rangle \cdot \left(Sc/_{660}\right)^{-0.5} \quad (3)$$

where the units of k_W are in cm h^{-1}, *Sc* is the dimensionless Schmidt number, and $\langle U^2 \rangle$ denotes the second moment of average 10-m height winds (m s^{-1}). We choose the quadratic dependence of the gas transfer velocity as it is widely accepted and used in the literature (Wanninkhof, 1992). Observational and modelling studies have often suggested that different parametrizations could be more appropriate under specific conditions (Fairaill et al., 2000; Nightingale et al., 2000; McGillis et al., 2001; Krakauer et al., 2006); however, recent direct carbon dioxide flux measurements made in the high latitude Southern Ocean confirm that even in this high wind environment, a quadratic parameterization fits the observations best (Butterworth and Miller, 2016). Future updates of the SeaFlux product will include options for other parameterizations. We calculate the square of the wind speed at the native resolution of each wind product and then average it to 1° by 1° monthly resolution. The order of this calculation is important as information is lost when resampling data to lower resolutions because of the concavity of the quadratic function. For example, if the second moment were calculated from time-averaged wind speeds, it would result in an underestimate of the gas transfer velocity (Sarmiento and Gruber 2006; (Sweeney et al., 2007). The resulting second moment is equivalent to $\langle U^2 \rangle = U_{mean}^2 + U_{std}^2$ where U_{mean} and U_{std} are the temporal mean and standard deviation calculated from the native temporal resolution of U.

In addition to the choice of wind parameterization, large differences in flux can result due to the scaling coefficient of gas transfer (*a*) that is applied when calculating the global mean piston velocity. This constant originates from the gas exchange process studies (Krakauer et al., 2006; Sweeney et al., 2007; Müller et al., 2008; Naegler, 2009) utilise observations of radiocarbon data from the GEOSECS and WOCE/JGOFS expeditions (Key et al., 2004). The ^{14}C released from nuclear bomb testing (hence bomb-^{14}C) in the mid twentieth century has since been taken up by the ocean. The number of bomb-^{14}C atoms in the ocean, relative to the pre-bomb ^{14}C, can thus be used as a constraint on the long-term rate of exchange of carbon between the atmosphere and the ocean. A probability distribution of wind speed is used to optimise the coefficient of gas transfer based on these observed natural and bomb ^{14}C invasion rates. This coefficient must be individually calculated and is not consistent for each wind product. Further, the gas transfer velocity used by the different pCO_2 mapping products are not scaled to the same bomb-^{14}C estimate. The range of the different bomb-^{14}C estimates is within the range of the uncertainty from the associated studies (Naegler, 2009), but the choice would introduce inconsistency that is easily addressed here.

We scale the gas transfer velocity to a bomb-^{14}C flux estimate of 16.5 cm hr^{-1} as recommended by Naegler, (2009). The coefficient (*a*) is calculated for each wind product via a cost function which optimises the coefficient of gas transfer

$$a = k_W \cdot \langle U^2 \rangle^{-1} \cdot \left(Sc/_{660}\right)^{0.5} \cdot (1 - ice) \quad (4)$$

where parameters are as defined in Equation 3. The units of the coefficient a are (cm h^{-1}) (m s^{-1})$^{-2}$. Global winds from the wind speed products differ and therefore even with the same bomb-^{14}C observations the scaled coefficient (a) can have a 40% range (Wanninkhof, 2014). By determining the optimal a coefficient

for each of the reanalysis winds, uncertainty in the global fluxes can be decreased. Our scaled coefficients correspond well with the estimate of Wanninkhof, (2014) who uses the CCMP wind product to estimate a as 0.251. Differences in the coefficient will also result from the time period considered and definition of global area and ice fraction applied in the calculation.

This scaling of the gas exchange coefficient (a) for each wind product is an essential, and an inconsistently applied step, that has large implications for air-sea flux estimates. Without individual scaling, and instead utilising a set value for the gas transfer coefficient (a) regardless of wind product, our results show that calculated global fluxes could be as high as 9% different depending on which pCO_2 and wind reanalysis product considered (Roobaert et al., 2018).

Step 4: Further parameters for flux calculation

The remaining parameters of Equation 1 are the solubility of CO_2 in seawater (*sol*), the atmospheric partial pressure of CO_2 (pCO_2^{atm}), and the area weighting to account for sea ice cover. While the choices of products used for these parameters can also result in differences in flux estimates, the impacts are much smaller as compared with the parameters discussed above.

Atmospheric pCO_2 is calculated as the product of surface xCO_2 and sea level pressure corrected for the contribution of water vapor pressure. The choice of the sea level pressure product, or absence of the water vapor correction can have small, but not insignificant, impact on the calculated fluxes. Additionally, some products utilise the output of an atmospheric CO_2 inversion product (e.g. CarboScope, (Rödenbeck et al., 2013), CAMS CO_2 inversion) (Chevallier, 2013) which can introduce differences in the flux estimate outside of the sources related to a product's surface ocean pCO_2 mapping method. Importantly, we do not advocate that our estimate of pCO_2^{atm} is an improvement over other estimates thereof; rather we provide an estimate of pCO_2^{atm} that has few assumptions and leads to a methodologically consistent estimate of ΔpCO_2. We maintain the same philosophy in our estimates of solubility of CO_2 in seawater and sea-ice area weighting and therefore we do not elaborate on them here.

5.SM.3 Biogeophysical sequestration potential of ocean-based CDR methods

Ocean fertilisation (OF) aims to boost primary production and subsequently organic carbon export by seeding the ocean surface with nutrients, typically in iron-limited areas such as the Southern Ocean or North Pacific. Iron fertilisation experiments have been inconclusive on whether deep-sea carbon sequestration is enhanced (Boyd et al., 2007; Yoon et al., 2018), with only one observing an increase in the biological pump below 1000 m (Smetacek et al., 2012), suggesting that the effectiveness of ocean fertilisation is low (*medium confidence*). Model simulations (Oschlies et al., 2010; Keller et al., 2014) suggest that if ocean fertilisation is applied continuously in the Southern Ocean under high CO_2 emission scenarios, CO_2 sequestration rates are initially between 2 and 4 PgC yr^{-1}, but then decrease to 0.4 to 1 PgC yr^{-1} after the initial decade, with an 80-year cumulative carbon uptake of 73 to 90 PgC. Taking the sequestration rates from these model simulations to constitute an upper limit, we assess the maximum biogeophysical sequestration potential of iron fertilization to be 1 PgC yr^{-1} (*low confidence*). Increased productivity in the fertilised areas would result in decreased productivity in unfertilised regions (Oschlies et al., 2010b). The carbonate counter pump could also reduce iron fertilisation-induced carbon sequestration by 6–32% (Salter et al., 2014).

Artificial ocean upwelling (AOUpw) brings nutrient-rich water to the ocean surface to alleviate nutrient limitation of (near-) surface phytoplankton growth and thus boost primary production and subsequent ocean CO_2 uptake. For AOUpw to be effective at increasing ocean carbon storage, the increased primary production has to result in increased transfer of organic carbon into the deep ocean. AOUpw also returns previously-sequestered dissolved inorganic carbon to the surface ocean, thus increasing surface water pCO_2 and decreasing (or potentially negating) atmospheric CO_2 drawdown stimulated by the additional nutrient input. In model simulations (Oschlies, 2010; Keller et al., 2014) where AOUpw is applied continuously and at the largest feasible scales, atmospheric CO_2 removal is up to 4.3 PgC yr^{-1} during the first decade, and decreases afterwards to 0.9 to 1.5 PgC yr^{-1} (average), with an 80-year cumulative CO_2 removal of 80 to 140

PgC. 50–80% of this removal results from cooling-induced enhancement of the terrestrial carbon sink (Keller et al., 2014). Removing terrestrial CO_2 removal from the total cumulative CO_2 removal yields cumulative ocean CO_2 removal of 16 to 70 PgC over 80 years, or 0.2 to 0.9 PgC yr^{-1} (*low confidence*).

Ocean alkalinisation, via the deposition of alkaline minerals (e.g. olivine) or their dissociation products (e.g. quicklime) at the ocean surface, can increase surface total alkalinity and thus increase CO_2 uptake and storage. Modelling studies suggest that massive additions of alkalinity (114 Pmol by the end of the century) in high CO_2 emission scenarios could increase ocean uptake by up to 27 PgC yr^{-1} by the end of the century (cumulative atmospheric CDR of up to 905 PgC), and permanently keep it there (100 ka residence time; Renforth & Henderson, 2017) even if additions were stopped (González et al., 2016; Feng et al., 2017; Sonntag et al., 2018). Taking the sequestration rates from these model simulations to constitute an upper limit, we assess the maximum biogeophysical sequestration potential of ocean alkalinisation to be 10 PgC yr^{-1} *(medium confidence*).

[START FIGURE 5.SM.1 HERE]

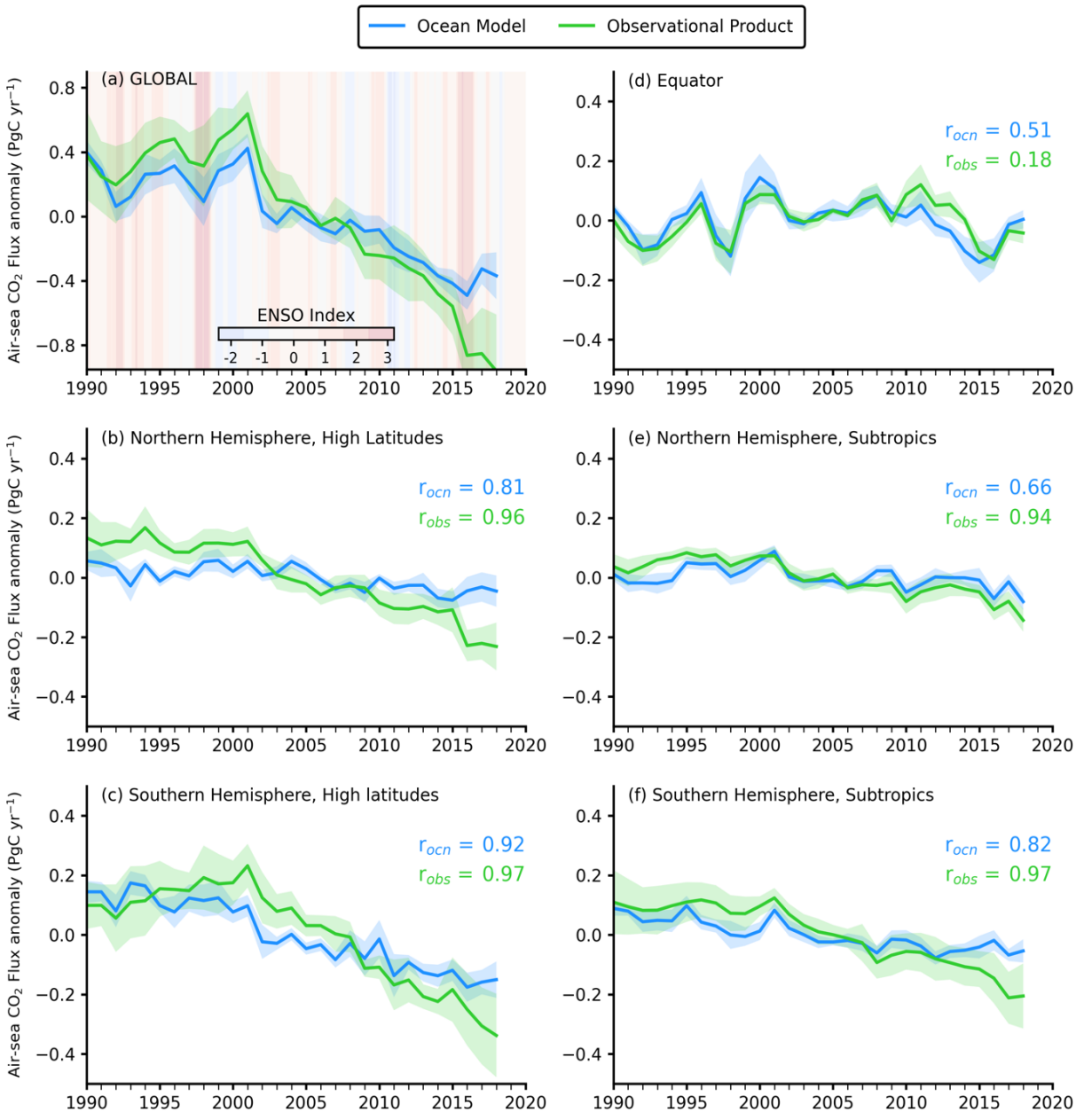

Figure 5.SM.1: A comparative assessment of the contribution made by 5 regional ocean biomes (panels b-f) to the temporal variability characteristics of the global mean air-sea CO_2 flux anomalies for the period 1990–2018 using ensembles of global ocean biogeochemical models (GOBMs; 9 time series), observation-based products (6 time series) (Gregor et al., 2019; Supplementary Material 5.SM.2) (based on the SOCATv6 observational data (Bakker et al., 2020). Numbers in the top right of panels (b) to (f) indicate the correlation between the regional mean time series of the different models and the global mean time series (panel a). The 5 regional super-biomes (boundaries in Figure 5.9a) were derived by aggregation of the original 17 biomes of Fay and McKinley (2014).

[END FIGURE 5.SM.1 HERE]

[START TABLE 5.SM.1 HERE]

Table 5.SM.1: Decadal mean for the global ocean sink (S_{ocean}) for anthropogenic CO_2 (PgC yr^{-1}) from global ocean biogeochemistry models, pCO_2 observation-based data products, and atmospheric CO_2 inverse models. The uncertainty range for the mean of each approach is 90% confidence intervals. The range of ocean CO_2 uptake for each models or products represents interannual variability.

Methods	1990-1999		2000-2009		2009-2018		2010-2019		Citation
Global ocean biogeochemistry models	**-1.96**	**± 0.48**	**-2.14**	**± 0.54**	**-2.48**	**± 0.56**	**-2.51**	**± 0.56**	
CESM-ETH	-1.81	± 0.26	-1.98	± 0.37	-2.30	± 0.26	-2.35	± 0.29	Doney et al., 2009
CSIRO	-2.45	± 0.27	-2.74	± 0.40	-3.10	± 0.24	-3.14	± 0.23	Law et al., 2017
FESOM-1.4-REcoM2	-1.73	± 0.22	-1.80	± 0.34	-2.13	± 0.36	-2.18	± 0.30	Hauck et al., 2020
MPIOM-HAMOCC6	-1.67	± 0.19	-1.94	± 0.26	-2.23	± 0.26	-2.25	± 0.26	Paulsen et al., 2017
NEMO3.6-PISCESv2-gas (CNRM)	-1.90	± 0.27	-1.92	± 0.27	-2.27	± 0.22	-2.31	± 0.25	Berthet et al., 2019
NEMO-PlankTOM5	-2.14	± 0.25	-2.29	± 0.27	-2.67	± 0.23	-2.71	± 0.20	Buitenhuis et al., 2013
MICOM-HAMOCC (NorESM-OCv1.2)	-2.39	± 0.20	-2.60	± 0.24	-2.91	± 0.28	-2.95	± 0.24	Schwinger et al., 2016
MOM6-COBALT (Princeton)	-1.74	± 0.23	-1.97	± 0.43	-2.35	± 0.24	-2.39	± 0.20	Liao et al., 2020
NEMO-PISCES (IPSL)	-1.85	± 0.26	-2.05	± 0.32	-2.35	± 0.31	-2.35	± 0.31	Aumont et al., 2015
p*CO_2 observation-based data products	**-1.89**	**± 0.37**	**-2.06**	**± 0.20**	**-2.62**	**± 0.32**			
MPI_SOMFFN	-1.74	± 0.23	-1.93	± 0.38	-2.54	± 0.11			Landschützer et al., 2014
JENA_MLS	-1.96	± 0.23	-2.12	± 0.31	-2.52	± 0.19			Rödenbeck et al., 2014
LSCE_FFNN2	-1.77	± 0.05	-1.94	± 0.18	-2.46	± 0.28			Denvil-Sommer et al., 2019
CSIR_ML6	-1.74	± 0.08	-2.01	± 0.24	-2.57	± 0.20			Gregor et al., 2019
NIES_NN	-1.80	± 0.10	-2.14	± 0.26	-3.00	± 0.44			Zeng et al., 2014
JMA_MLR	-2.31	± 0.16	-2.24	± 0.17	-2.66	± 0.29			Iida et al., 2020
Atmospheric CO_2 inverse models*			**-2.13**	**± 0.47**	**-2.36**	**± 0.72**	**-2.40**	**± 0.74**	
MIROC4-lr2020			-1.97	± 0.27	-1.91	± 0.45	-1.90	± 0.45	Saeki and Patra, 2017
MIROC4-gcp2020			-1.90	± 0.30	-2.10	± 0.27	-2.18	± 0.31	Saeki and Patra, 2017
CAMS2020			-2.12	± 0.11	-2.54	± 0.23	-2.60	± 0.24	Chevallier et al., 2005
CTE2020			-2.54	± 0.46	-2.88	± 0.29	-2.91	± 0.26	van der Laan-Luijkx et al., 2017
Previous IPCC assessment reports									
TAR	-1.7	± 0.8							Prentice et al., 2001
AR4	-2.2	± 0.7							Denman et al., 2007
AR5	-2.2	± 0.7	-2.3	± 0.7					Ciais et al., 2013

***** Pre-industrial sea-to-air CO_2 flux associated with land-to-ocean carbon flux of +0.62 PgC $year^{-1}$ (Jacobson et al., 2007; Resplandy et al., 2018) has been subtracted from original flux estimates.

[END TABLE 5.SM.1 HERE]

[START TABLE 5.SM.2 HERE]

Table 5.SM.2: Decadal means for the global ocean sink (S_{ocean}) for anthropogenic CO_2 (PgC yr^{-1}) from methods additional to those show in Table 5.SM.1. The uncertainty ranges presented here are 90% confidence intervals otherwise specified.

Methods	Citation	Period	Sea-to-air flux		Global ocean biogeochemistry models		pCO_2 observation-based data products	Atmospheric CO_2 inverse models
Ocean interior carbon inventory change	Gruber et al., 2019a	1994-2007	-2.23	± 0.31	-2.05	± 0.50	-1.93 ± 0.27	-1.99 ± 0.20
Ocean interior CFC inventory change	McNeil et al., 2003	1980-1989	-1.6	± 0.4 *	-1.71	± 0.48		
		1990-1999	-2.0	± 0.4 *	-1.96	± 0.48	-1.89 ± 0.37	
Ocean interior $\Delta^{14}C$ change and GOBMs	Graven et al., 2012	1990-2007	-2.0	± 0.3 *	-2.03	± 0.50	-1.94 ± 0.30	
Ocean inverse model	Gloor et al., 2003	1990	-1.80	± 0.40 *	-1.79	± 0.54	-1.87 ± 0.60	
	Mikaloff Fletcher et al., 2006; Gruber et al., 2009	1995-2000	-2.2	± 0.41	-1.94	± 0.47	-1.81 ± 0.34	-2.02 ± 0.04
	DeVries et al., 2017	1990-1999	-1.25	± 0.53	-1.96	± 0.48	-1.89 ± 0.37	
		2000-2014	-2.41	± 0.20	-2.24	± 0.55	-2.20 ± 0.19	-2.21 ± 0.35
Joint atmosphere-ocean inversion	Jacobson et al., 2007	1992-1996	-2.1	± 0.2	-1.99	± 0.45	-1.88 ± 0.33	
Deconvolution atm. $\delta^{13}C$ and CO_2	Joos et al., 1999	1985-1995	-2.0	± 1.3	-1.84	± 0.49		
Atmospheric O_2/N_2 ratio & $\delta^{13}C$	Battle et al., 2000	1991-1997	-2.0	± 0.6 *	-1.97	± 0.47	-1.90 ± 0.35	
Air-sea $\delta^{13}C$ disequilibrium	Gruber and Keeling, 2001	1985-1995	-1.5	± 0.9 *	-1.84	± 0.49		
Atmospheric O_2/N_2 ratio	Bender et al., 2005	1994-2002	-1.70	± 0.50 *	-1.95	± 0.48	-1.81 ± 0.31	-2.01 ± 0.06
	Keeling and Manning, 2014	1990-2000	-1.94	± 1.02	-1.95	± 0.48	-1.87 ± 0.36	
		1993-2003	-2.20	± 0.94	-1.98	± 0.48	-1.85 ± 0.30	-1.96 ± 0.13
		2000-2010	-2.72	± 0.99	-2.16	± 0.54	-2.09 ± 0.19	-2.12 ± 0.31
	Tohjima et al., 2019	1991-2011	-2.45	± 0.96	-2.09	± 0.51	-2.02 ± 0.24	
		1999-2003	-2.20	± 1.20	-1.99	± 0.52	-1.82 ± 0.33	-2.06 ± 0.11
		2004-2008	-1.97	± 1.02	-2.22	± 0.57	-2.18 ± 0.19	-2.17 ± 0.45

2009-2013	-2.65 ± 1.44	-2.37 ± 0.56	-2.43 ± 0.24	-2.26 ± 0.48
2012-2016	-3.05 ± 1.49	-2.55 ± 0.57	-2.63 ± 0.33	-2.40 ± 0.39

[END TABLE 5.SM.2 HERE]

[START TABLE 5.SM.3 HERE]

Table 5.SM.3: Compiled information on the rates of pH change and aragonite saturation state (Ω_{arag}) change from various time series, ship reoccupations and moorings.

Station, region	Study period	pH change (per decade)	Uncer-tainty	Ω_{arag} change (per decade)	Uncer-tainty	Study type	Citation
North Atlantic							
Iceland Sea (winter) (68°N, 12.67°W)	1985-2008	-0.024	±0.002	-0.072	±0.007	Time series	Olafsson et al., 2009
	1985-2010	-0.014	±0.005	-0.018	±0.027		Bates et al., 2014
Irminger Sea (64.3°N, 28°W)	1983-2004	-0.026	±0.006	-0.08	±0.04	Time series	Bates et al., 2014
Subpolar Gyre	1981-2007	-0.022	±0.004			Merged ship occupations	Lauvset and Gruber, 2014
NA-SPSS	1991-2011	-0.02	±0.004			Merged ship occupations	Lauvset et al., 2015
NA-STSS	1991-2011	-0.018	±0.003			Merged ship occupations	Lauvset et al., 2015
BATS (32°N, 64°W)	1983-2010	-0.018	±0.002	-0.11	±0.01	Time series	Takahashi et al., 2014
	1983-2012	-0.017	±0.001	-0.095	±0.007		Bates et al., 2014
	1983-2020	-0.019	±0.001	-0.09	±0.01		Bates and Johnson, 2020
ESTOC (29.04°N, 15.50°W)	1995-2004	-0.017	±0.003			Time series	González-Dávila et al., 2010
	1995-2011	-0.018	±0.002	-0.115	±0.023		Bates et al., 2014
	1996-2010	-0.02	±0.004	-0.1	±0.02		Takahashi et al., 2014
NA-STPS	1991-2011	-0.011	±0.002			Merged ship occupations	Lauvset et al., 2015
CARIACO (10.50°N, 64.66°W)	1995-2012	-0.025	±0.004	-0.066	±0.028	Time series	Bates et al., 2014
Mediterranean							
Dyfamed (43.42°N, 7.87°E)	1995-2011	-0.03	±0.01			Time series	Yao et al., 2016

GIFT, Gibraltar	2012-2015	-0.044	±0.006			Time series	Flecha et al., 2019
Equatorial Atlantic							
A-EQU	1991-2011	-0.016	±0.003			Merged ship occupations	Lauvset et al., 2015
South Atlantic							
SA-STPS	1991-2011	-0.011	±0.005			Merged ship occupations	Lauvset et al., 2015
Atlantic Meridional Transect (50S-50N)	1995-2013	-0.013	±0.009			Merged ship occupations	Kitidis et al., 2017
North Pacific							
NP-SPSS	1983-2011 1991-2011	-0.003 0.013	±0.005 ±0.005			Merged ship occupations	Lauvset et al., 2015
Papa (50°N, 145°W)	2007-2014	-0.01	±0.005	0.1	0.04	Mooring	Sutton et al., 2017
K2 (47°N, 160°E) (Winter)	1999-2015	-0.025 -0.008	±0.01 ±0.004	-0.12	0.05	Time series	Wakita et al., 2017
NP-STSS	1991-2011	-0.01	±0.005			Merged ship occ	Lauvset et al., 2015
HOT (22.75°N, 158°W)	1988-2007 1988-2009 1988-2011	-0.019 -0.018 -0.016	±0.002 ±0.001 ±0.001	 -0.08 -0.084	 ±0.01 ±0.011	Time series	Dore et al., 2009 Takahashi et al., 2014 Bates et al., 2014
WHOTS (23°N, 158°W)	2004-2013	-0.02	±0.003	-0.2	±0.02	Mooring	Sutton et al., 2017
KEO (32°N, 144°E)	2007-2014	-0.01	±0.005	-0.1	±0.02	Mooring	Sutton et al., 2017
137°E Line 33°N-34°N	1994-2008	-0.020	±0.007	-0.12	±0.05	Merged ship occupations	Ishii et al., 2011
137°E Line 26°N-30°N	1983-2017	-0.0193	±0.0008	-0.121	±0.005	Merged ship occupations	Ono et al., 2019
137°E Line 20°N-22°N		-0.0171	±0.0007	-0.113	±0.004		
137°E Line 11°N-18°N		-0.0136	±0.0007	-0.09	±0.005		
137°E Line 5°N-10°N		-0.0124	±0.0008	-0.081	±0.005		
NP-STPS	1983-2011 1991-2011	-0.016 -0.019	±0.002 ±0.002			Merged ship occupations	Lauvset et al., 2015
Equatorial Pacific							
WP-EQU	1983-2011 1991-2011	-0.01 -0.012	±0.002 ±0.002			Merged ship occupations	Lauvset et al., 2015
Warm Pool in 130°E-180°	1985-2016	-0.013	±0.001	-0.083	±0.007	Merged ship occupations	Ishii et al., 2020

EP-EQU		1983-2011 1991-2011	-0.023 -0.026	±0.003 ±0.002			Merged ship occupations	Lauvset et al., 2015
TAO	0°, 155°W 0°, 140°W 0°, 125°W	1997-2011 2004-2011 2004-2011	-0.022 -0.018 -0.026	±0.003 ±0.004 ±0.005			Moorings	Sutton et al., 2014
South Pacific								
Munida (45.833°S, 171.5°E)		1998-2011	-0.013	±0.003	-0.085	±0.026	Time series	Bates et al., 2014
SP-STPS		1983-2011 1991-2011	-0.019 -0.022	±0.002 ±0.003			Merged ship occupations	Lauvset et al., 2015
Stratus (20°S, 86°W)		2006-2015	-0.02	±0.003	-0.1	±0.03	Merged ship occupations	Sutton et al., 2017
Indian Ocean								
East Eq. Indian (90°E-95°E)		1962-2012	-0.016	±0.001	-0.095	±0.005	Merged ship occupations	Xue et al., 2014
IO-STPS		1987-2011 1991-2011	-0.024 -0.027	±0.004 ±0.005			Merged ship occupations	Lauvset et al., 2015
Southern Ocean								
140°E-160°E	North of STF SAZ PFZ PZ	1969-2003	-0.011 -0.011 -0.013 -0.020	±0.004 ±0.004 ±0.003 ±0.003			Merged ship occupations	Midorikawa et al., 2012
Drake Passage	SAZ PZ	2002-2012	-0.023 -0.015	±0.007 ±0.008	-0.09 -0.06	±0.05 ±0.05	Merged ship occupations	Takahashi et al., 2014
SO-STSS		1983-2011 1991-2011	-0.006 -0.004	±0.004 ±0.004			Merged ship occupations	Lauvset et al., 2015
SO-SPSS		1983-2011 1991-2011	-0.02 -0.021	±0.002 ±0.002			Merged ship occupations	Lauvset et al., 2015
PAL-LTER, west Antarctic Peninsula		1993-2012	0.02	±0.02	0.01	±0.1	Time series	Hauri et al., 2015
SO-ICE		1991-2011	-0.002	±0.004			Merged ship occupations	Lauvset et al., 2015

[END TABLE 5.SM.3 HERE]

[START TABLE 5.SM.4 HERE]

Table 5.SM.4: Explanation and references of earth system feedbacks, biogeochemical and biophysical impacts, and trade-offs and co-benefits of the carbon dioxide removal (CDR) methods as presented in Figure 5.37.

CDR Method	Earth system feedbacks on CO_2 sequestration potential and temperature	Biogeochemical and biophysical effects	Trade-offs and co-benefits related to water quantity and quality, food supply, biodiversity (BD)
Afforestation, reforestation and forest management	Weakens ocean C sequestration through decreased [CO_2] (Keller et al., 2018; Sonntag et al., 2018); decrease in albedo due to afforestation weakens the effect of CO_2 removal on surface air temperature (Sonntag et al., 2018); may shift the location of the Intertropical Convergence Zone and hence precipitation in the monsoon regions (Devaraju et al., 2015a)	Increased emissions of biogenic volatile organic compounds (BVOC) (Krause et al., 2017, SRCCL Sections 2.5.2.1, 2.6.1.2), decreased and increased surface temperature, in tropics and boreal region, respectively, due to changes in albedo, evapotranspiration and surface roughness (SRCCL Section 2.5.2.1; Fuss et al., 2018; Griscom et al., 2017; Pongratz et al., 2010; Jackson et al., 2008; Bright et al., 2015; Devaraju et al., 2015); decreased (Chen et al., 2019; Zhou et al., 2019; Deng et al., 2019) or increased (Benanti et al., 2014) N_2O emissions; increased CH_4 uptake (Chen et al., 2019; Nisbet et al., 2020)	Threatened water supply in dry areas regional climate, initial land cover, and scale of deployment (Farley et al., 2005; Mengis et al., 2019); improved water quality due to higher soil water retention and filtering capacity (Smith et al., 2019); affects food supply through competition for land (Smith et al., 2018b); decreased BD if not adopted wisely, increased BD if monocultures are replaced by native species (Smith et al., 2018; Williamson & Bodle, 2016); potentially negative impacts on food security due to land requirements (Smith et al., 2020).
Soil carbon sequestration	Weakens ocean C sequestration through decreased [CO_2] (Keller et al., 2018)	Decreased or increased N_2O emissions, depending on management strategy, fertilization, land-use, use of cover crops (Smith et al., 2016; Gu et al., 2017; Fuss et al., 2018b) Small or negligible impact on soil CH_4 flux (Smith et al., 2008); Albedo increase by no-till farming (Davin et al., 2014)	Reduced nutrient losses, increased biological activity (Fornara et al., 2011; Paustian et al., 2016; Tonitto et al., 2006; (Fuss et al., 2018b; Smith, 2016), improved soil water holding capacity (Paustian et al., 2019), positive impact on food security due to increased yield (Smith et al., 2020); no impact or increased BD, depending on method (Paustian et al., 2016; Smith et al., 2018b)
Biochar	Weakens ocean C sequestration through decreased [CO_2] (Keller et al., 2018)	Decreased N_2O emissions (Cayuela et al., 2014; Kammann, 2017), decreased CH_4 uptake in non-inundated soils (Jeffery et al., 2016); decreased CH_4 emissions in inundated soils such as rice fields (Jeffery et al., 2016; Yang et al., 2019; Wang et al., 2019; Huang et al., 2019), local warming related to darkened surface (Genesio et al., 2012; Zhang et al., 2018; Jia et al., 2019, SRCCL); VOC's	Improved soil fertility and productivity, reduced nutrient losses, enhanced fertiliser N use efficiency (Clough et al., 2013; Liu et al., 2017; Shen et al., 2016, Woolf et al., 2010); improved soil water holding capacity (Karhu et al., 2011; Verheijen et al., 2019; C. Liu et al., 2016; Bock et al., 2017; Fischer et al., 2019); no impact or increased BD (Smith et al., 2018); adverse impacts on BD due to land

		produced when preparing biochar can be toxic to plants and animals (Buss and Mašek, 2016)	requirements of feedstock (12.3.3, WGIII); benefits for food security due to improved yields (Smith et al., 2020)
Peatland restoration	no evidence	Enhanced CH_4 emission (Vanselow-Algan et al., 2015; Wilson et al., 2016; Renou-Wilson et al., 2019; Hemes et al., 2019; Holl et al., 2020); suppressed N_2O emissions (Wilson et al., 2016; Liu et al., 2020; Tiemeyer et al., 2020); increased (Koskinen et al., 2017) or decreased (Singh et al., 2019) leaching of nutrients; surface cooling due to higher evapotranspiration (Hemes et al., 2018; Helbig et al., 2020; Worrall et al., 2019)	Increased nutrient infiltration and retention to increase water quality (Daneshvar et al., 2017; Kluber et al., 2014; Lundin et al., 2017); protection from fire, increased BD (Meli et al., 2014; Smith et al., 2018b)
Restoration of vegetated coastal ecosystems (‘blue carbon’)	no evidence	Emission of CH_4 and N_2O, and biogenic calcification may partly offset benefits (Rosentreter et al., 2018; Keller, 2019; Kennedy et al., 2019)	Provision of very wide range of ecosystem services (biodiversity support recreation and tourism; fishery habitats; improved water quality, and flood and erosion protection) (Bindoff et al., 2019)
Ocean fertilisation	Carbonate counter pump could decrease C sequestration (Salter et al., 2014); Weakens terrestrial C storage (Keller et al., 2018)	Enhanced subsurface ocean acidification (Cao and Caldeira, 2010; Williamson et al., 2012a; Oschlies, 2009); Increased suboxic zone extent in fertilised areas; Shrinkage of suboxic zones outside fertilised areas (Oschlies, 2009; Keller et al., 2014); Increased production of N_2O and CH_4 (Jin and Gruber, 2003; Lampitt et al., 2008)	Perturbation to marine ecosystems via reorganisation of community structure, including possibly toxic algal blooms (Oschlies et al., 2010a; Williamson et al., 2012)
Artificial ocean upwelling	Cooling effect; increases terrestrial C storage (Oschlies et al., 2010b; Keller et al., 2014; Kwiatkowski et al., 2015); Returns previously sequestered C to ocean surface, decreasing or potentially negating CO_2 drawdown (Bauman et al., 2014; Kwiatkowski et al., 2015)	Enhanced subsurface ocean acidification (Cao and Caldeira, 2010; Oschlies et al., 2010c; Williamson et al., 2012a); Increased suboxic zone extent in fertilised areas (Keller et al., 2014; Feng et al., 2020); alters ocean temperature, salinity, circulation (Keller et al., 2014b); alters Earth’s heat and water budget (Keller et al., 2014); increased production of N_2O and CH_4 (Jin and Gruber, 2003; Lampitt et al., 2008; Williamson et al., 2012a)	Perturbation to marine ecosystems via reorganisation of community structure, including possibly toxic algal blooms (Oschlies et al., 2010a; Williamson et al., 2012)
Ocean alkalinisation	Increased ocean C storage through enhanced primary production through addition of iron and silicic acid from olivine dissolution (Köhler	Decreased ocean acidification (surface waters only); decreased de-oxygenation (González and Ilyina, 2016)	Release of toxic trace metals from some deposited minerals (Hartmann et al., 2013) Perturbation to marine ecosystems via

	et al., 2013; Hauck et al., 2016); Lowers terrestrial carbon storage (González and Ilyina, 2016; Sonntag et al., 2018)		reorganisation of community structure (González and Ilyina, 2016; González et al., 2018)
Enhanced weathering - terrestrial	Will initially reduce the ocean CO_2 sequestration, but after enough weathering products are transported into ocean to increase alkalinity, will increase ocean CO_2 sequestration (Keller et al., 2018)	Decreased N_2O emissions (Blanc-Betes et al; Kantola et al., 2017); reduced ocean acidification (Beerling et al., 2018)	Soil fertilisation and stimulated biological production (Hartmann et al., 2013); can liberate toxic trace metals into soil or water bodies (Keller et al., 2018); can decrease drinking water quality by causing freshwater salinization (Kaushal et al., 2018); increases alkalinity and pH of natural waters (Beerling et al., 2018); adverse impact on BD from mining (Smith et al., 2018)
BECCS	Weakens ocean C sequestration through decreased [CO_2] (Keller et al. 2018); Can weaken or strengthen land C sequestration depending on whether bioenergy crops replace marginal land or carbon-rich ecosystems (Don et al., 2012; Heck et al., 2016; Boysen et al., 2017a,b) (Harper et al., 2018)	Increased N_2O emissions related to land-use or if fertilized (Creutzig et al., 2015; Smith et al., 2016); local warming due to decreased albedo depending on the type of bioenergy crop (Smith et al., 2016); VOC emissions (Krause et al., 2017)	Threatened water supply (Farley et al., 2005; Smith et al., 2016, Cross-chapter box 5.1); threatened food supply through competition for land (Smith et al., 2019); soil nutrient deficiency; decreased BD depending on scale and previous land-use (Smith et al., 2018; Creutzig et al., 2019; Heck et al., 2018); see DACCS for storage-related side effects
Direct air carbon capture and storage (DACCS)	Weakens ocean and land C sequestration through decreased [CO_2] (Tokarska and Zickfeld, 2015; Jones et al., 2016; Zickfeld et al., 2021)	No evidence or not applicable	Perturbation of marine ecosystems through leakage of CO_2 from submarine storage (Molari et al., 2018); potentially decreased BD due to land and water requirements (Williamson, P., & Bodle, 2016); water use or production (Fuss et al., 2018; NASEM, 2019); VOC emissions in solid-sorbent systems (NASEM, 2019); Storage related: pollution of drinking water; seismic activity, leaks (Fuss et al., 2018)

[END TABLE 5.SM.4 HERE]

[START TABLE 5.SM.5 HERE]

Table 5.SM.5: Carbon dioxide removal (CDR) Potentials: Details underlying sequestration potentials classification shown in Figure 5.37.

CDR Method	Technical/ biogeophysical sequestration potential class*	Confidence level	Technical/ biogeophysical sequestration potential median and range**	Sequestration potential category	Data source
Afforestation, reforestation and forest management	Large	Medium (large evidence, medium agreement)	Afforestation, reforestation: 3.7 (0.5–10) $GtCO_2e\ yr^{-1}$; forest management 1.8 (1–2.1) $GtCO_2e\ yr^{-1}$	Technical potential; estimates also consider environmental and social factors	Median and range calculated based on technical and sustainable potentials from (Roe et al., 2019a)
Soil carbon sequestration	Moderate	Medium (large evidence, medium agreement)	Croplands: 1.6 (0.4–6.8) $GtCO_2e\ yr^{-1}$; Pasture lands: 0.7 (0.15–2.6) $GtCO_2e\ yr^{-1}$	Technical potential; estimates also consider environmental and social factors	Median and range calculated based on technical and sustainable potentials from (Roe et al., 2019b)
Biochar	Moderate	Medium (medium evidence, medium agreement)	1.1 (0.1–4.9) $GtCO_2e\ yr^{-1}$	Technical potential; estimates also consider environmental and social factors	Median and range calculated based on technical and sustainable potentials from (Roe et al., 2019b)
Peatland restoration	Moderate	Low (low evidence)	0.7 (0.6–0.8) $GtCO_2e\ yr^{-1}$	Technical potential; estimates also consider environmental and social factors	Median and range calculated based on technical and sustainable potentials from (Roe et al., 2019b)
Restoration of vegetated coastal ecosystems (‘blue carbon’)	Low	Low (low evidence)	0.2–0.7 $GtCO_2\ yr^{-1}$ (0.05–0.2 $GtC\ yr^{-1}$); 0.2–0.8 $GtCO_2\ yr^{-1}$	Technical potential; estimates also consider environmental and social factors	SROCC Ch 5 (IPCC, 2019); Range calculated based on technical and sustainable potentials from (Roe et al., 2019b)
Ocean iron fertilization	Large	Low (medium evidence, low agreement)	<3.7 $GtCO_2\ yr^{-1}$ (<1 $GtC\ yr^{-1}$); 3.7 $GtCO_2\ yr^{-1}$ (1 $GtC\ yr^{-1}$); 3.7 (0–44) $GtCO_2\ yr^{-1}$	Biogeophysical potential	Supplementary Material 5.SM3; (GESAMP, 2019) Table 4.4; median and range based on global studies considered in (Fuss et al., 2018)

Artificial ocean upwelling	Moderate	Low (low evidence)	0.7–3.3 $GtCO_2\ yr^{-1}$ (0.2–0.9 GtC yr^{-1}); <0.7 $GtCO_2\ yr^{-1}$ (< 0.2 GtC/yr)	Biogeophysical potential	Supplementary Material 5.SM3; (GESAMP, 2019) Table 4.4
Ocean alkalinization	Large	Medium (medium evidence, medium agreement)	<37 $GtCO_2\ yr^{-1}$ (<10 GtC yr^{-1}); 3.7 $GtCO_2\ yr^{-1}$ (1 GtC yr^{-1}); 1–99 $GtCO_2\ yr^{-1}$	Biogeophysical potential	Supplementary Material 5.SM3; (GESAMP, 2019) Table 4.4; full range (Fuss et al., 2018)
Enhanced weathering	Large	Medium (medium evidence, low agreement)	3.7 (1–95) $GtCO_2\ yr^{-1}$	Technical potential	Median and range based on global studies considered in (Fuss et al., 2018)
BECCS	Large	Medium (medium evidence, medium agreement)	4.6 (0.4–11.3) $GtCO_2\ yr^{-1}$	Technical potential; estimates also consider environmental and social factors	Median and range calculated based on technical and sustainable potentials from (Roe et al., 2019b)
DACCS	Large	Medium (low evidence, large agreement)	5–40 $GtCO_2\ yr^{-1}$	Technical potential	Full range (Fuss et al., 2018)

*Potentials classes: Low <0.3 $GtCO_2\ yr^{-1}$; Moderate 0.3–3 $GtCO_2\ yr^{-1}$; Large >3 $GtCO_2\ yr^{-1}$; classification based on *median* potentials estimate

**WGIII will present an update of these estimates based on more recent literature

[END TABLE 5.SM.5 HERE]

5.SM.4 Data Table

[START TABLE 5.SM.6 HERE]

Table 5.SM.6: Input Data Table. Input datasets and code used to create chapter figures

Figure number / Table number / Chapter section (for calculations)	Dataset / Code name	Type	Filename / Specificities	License type	Dataset / Code citation	Dataset / Code URL	Related publications / Software used	Notes [Can add info on data processing, e.g., reference period conversion]
Figure 5.3 (a)	CO2, 60M year BCE	proxy CO2 reconstructions based on marine and terrestrial archives		Published	Chapter 2, AR6		(Foster et al., 2017)	
	CO2, 800k year BCE	ice air-bubble measurement	Ch2_ice_core.xlsx	Published	Chapter 2, AR6		(Bereiter et al., 2015)	
	CO2, 1-1749 year CE	ice air-bubble measurement		Published	Chapter 2, AR6		(Rubino et al., 2019)	
	CO2, 1750-2019	air-bubble & ambient air measurement	LLGHG_history_AR6_v9_updated.xlsx		Chapter 2, AR6		(Meinshausen et al., 2017)	Updated from Meinshausen et al. (2017) by Jinho Anh
	CO2, 2020-2100	model output		Published				
Figure 5.3 (b)	CO2, 60M year BCE	proxy CO2 reconstructions based on marine and terrestrial archives			Chapter 5, AR6		Python 3.8, for growth rate calculation	
	CO2, 800k year BCE	ice air-bubble measurement			Chapter 5, AR6		Python 3.8, for growth rate calculation	
	CO2, 1-1749 year CE	ice air-bubble measurement			Chapter 5, AR6		Python 3.8, for growth rate calculation	
	CO2, 1750-2019	air-bubble & ambient air			Chapter 5, AR6		Python 3.8, for growth rate	

		measurement					calculation	
	CO2, 2020-2100	model output			Chapter 5, AR6		Python 3.8, for growth rate calculation	
Figure 5.4 (a)	CO2, 800k year BCE	ice air-bubble measurement	Ch2_ice_core.xlsx		Chapter 2, AR6		(Foster et al., 2017) (Bereiter et al., 2015)	
	CO2, 1-1749 year CE	ice air-bubble measurement			Chapter 2, AR6		(Rubino et al., 2019)	
	CO2, 1750-2019	air-bubble & ambient air measurement	LLGHG_history_AR6_v9_updated.xlsx		Chapter 2, AR6		(Meinshausen et al., 2017)	Updated from Meinshausen et al. (2017) by Jinho Anh
					Chapter 5, AR6		Python 3.8, for growth rate calculation	
Figure 5.4 (b)	CH4, 800k year BCE	ice air-bubble measurement	Ch2_ice_core.xlsx		Chapter 2, AR6		(Loulergue et al., 2008)	
	CH4, 1-1749 year CE	ice air-bubble measurement			Chapter 2, AR6		(Rubino et al., 2019)	
	CH4, 1750-2019	air-bubble & ambient air measurement	LLGHG_history_AR6_v9_updated.xlsx		Chapter 2, AR6		(Meinshausen et al., 2017)	Updated from Meinshausen et al. (2017) by Jinho Anh
					Chapter 5, AR6		Python 3.8, for growth rate calculation	
Figure 5.4 (c)	N2O, 800k year BCE	ice air-bubble measurement	Ch2_ice_core.xlsx		Chapter 2, AR6		(Schilt et al., 2010)	
	N2O, 1-1749 year CE	ice air-bubble measurement			Chapter 2, AR6		(Rubino et al., 2019)	
	N2O, 1750-2019	air-bubble & ambient air measurement	LLGHG_history_AR6_v9_updated.xlsx		Chapter 2, AR6		(Meinshausen et al., 2017)	Updated from Meinshausen et al. (2017) by Jinho Anh
					Chapter 5, AR6		Python 3.8, for growth rate calculation	
Figure 5.5 (a)	Annual global CO2 (Land-use)	model-based estimation		Published			(Friedlingstein et al., 2020)	

	emissions							
	Annual global CO2 (fossil-fuel) emissions	emission inventory		Published			(Friedlingstein et al., 2020)	
Figure 5.5 (b)	Annual global CO2 emissions from land-use change	DGVM range					(Friedlingstein et al., 2020)	
	Annual global CO2 emissions from land-use change	DGVM mean					(Friedlingstein et al., 2020)	
	Annual global CO2 emissions from land-use change	BLUE					(Hansis et al., 2015)	
	Annual global CO2 emissions from land-use change	OSCAR					(Gasser et al., 2020)	
	Annual global CO2 emissions from land-use change	Bookkeeping					(Houghton and Nassikas, 2017)	
Figure 5.6 (a)	CO2, Mauna Loa	ambient air	monthly_flask_co2_mlo.csv		SIO/UCSD	Scripps CO2 Program (http://scrippsco2.ucsd.edu)	(Keeling et al., 2001)	
	CO2, South Pole	ambient air	monthly_flask_co2_spo.csv		SIO/UCSD	Scripps CO2 Program (http://scrippsco2.ucsd.edu)	(Keeling et al., 2001)	
	CO2, Global	Global, marine background air	co2_mm_gl.txt		GMD/NOAA	NOAA	(Conway et al., 1994)	
	CO2, GOSAT	total column dry air mole fractions	whole-atmosphere-monthly-mean_co2_january_2021.txt		NIES	NIES, https://www.gosat.nies.go.jp/en/recent-global-co2.html	(Yoshida et al., 2013)	

Figure 5.6 (b)	CO2, Mauna Loa	ambient air			Chapter 5, AR6		(Nakazawa et al., 1997)	Python 3.8, Nakazawa et al. (1997) for growth rate calculation
	CO2, South Pole	ambient air			Chapter 5, AR6		(Nakazawa et al., 1997)	Python 3.8, Nakazawa et al. (1997) for growth rate calculation
	CO2, Global	Global, marine background air			Chapter 5, AR6		(Nakazawa et al., 1997)	Python 3.8, Nakazawa et al. (1997) for growth rate calculation
	CO2, GOSAT	total column dry air mole fractions			Chapter 5, AR6		(Nakazawa et al., 1997)	Python 3.8, Nakazawa et al. (1997) for growth rate calculation
Figure 5.6 (c)	d13C-CO2 Mauna Loa	ambient air	monthly_flask_c13_mlo		SIO/UCSD	Scripps CO2 Program (http://scrippsco2.ucsd.edu)	(Keeling et al., 2001)	
	d13C-CO2 South Pole	ambient air	monthly_flask_c13_spo		SIO/UCSD	Scripps CO2 Program (http://scrippsco2.ucsd.edu)	(Keeling et al., 2001)	
	D14C-CO2 Wellington	ambient air	BHD_14CO2_datasets_20210309.xlsx		GNS Science/NIWA		(Turnbull et al., 2017)	
Figure 5.6 (d)	O2/N2 Mauna Loa	ambient air	mloav.csv		SIO/UCSD	Scripps O2 Program (http://scrippso2.ucsd.edu)	(Keeling and Manning, 2014)	
	O2/N2 South Pole	ambient air	spoav.csv		SIO/UCSD	Scripps O2 Program (http://scrippso2.ucsd.edu)	(Keeling and Manning, 2014)	
Figure 5.7	Anthropogenic		Dataset2020_Glo		GCP-CO2		(Friedlingstein et	

	emission, Fossil Fuel		bal_Budget_v1.0.xlsx				al., 2020)	
	Anthropogenic emission, Landuse change		Dataset2020_Global_Budget_v1.0.xlsx		GCP-CO2		(Friedlingstein et al., 2020)	
	CO2, 1750-2019	ambient air measurement	LLGHG_history_AR6_v9_updated.xlsx		Chapter 2, AR6		(Meinshausen et al., 2017)	Updated from Meinshausen et al. (2017) by Jinho Anh
	ENSO Index		meiv2.data				(Wolter and Timlin, 2011)	
Figure 5.8 (b)	CESM-ETH	Global ocean biogeochemistry model output	Global_Carbon_Budget_2020v1.0.xlsx		(Friedlingstein et al., 2020)	https://www.icos-cp.eu/science-and-impact/global-carbon-budget/2020	(Doney et al., 2009b)	
	CSIRO	Global ocean biogeochemistry model output	Global_Carbon_Budget_2020v1.0.xlsx		(Friedlingstein et al., 2020)	https://www.icos-cp.eu/science-and-impact/global-carbon-budget/2020	(Law et al., 2017)	
	FESOM-1.4-REcoM2	Global ocean biogeochemistry model output	Global_Carbon_Budget_2020v1.0.xlsx		(Friedlingstein et al., 2020)	https://www.icos-cp.eu/science-and-impact/global-carbon-budget/2020	(Hauck et al., 2020)	
	MPIOM-HAMOCC6	Global ocean biogeochemistry model output	Global_Carbon_Budget_2020v1.0.xlsx		(Friedlingstein et al., 2020)	https://www.icos-cp.eu/science-and-impact/global-carbon-budget/2020	(Paulsen et al., 2017)	
	NEMO3.6-PISCESv2-gas (CNRM)	Global ocean biogeochemistry model output	Global_Carbon_Budget_2020v1.0.xlsx		(Friedlingstein et al., 2020)	https://www.icos-cp.eu/science-and-impact/global-	(Berthet et al., 2019)	

						carbon-budget/2020		
	NEMO-PlankTOM5	Global ocean biogeochemistry model output	Global_Carbon_Budget_2020v1.0.xlsx		(Friedlingstein et al., 2020)	https://www.icos-cp.eu/science-and-impact/global-carbon-budget/2020	(Buitenhuis et al., 2013)	
	MICOM-HAMOCC (NorESM-OCv1.2)	Global ocean biogeochemistry model output	Global_Carbon_Budget_2020v1.0.xlsx		(Friedlingstein et al., 2020)	https://www.icos-cp.eu/science-and-impact/global-carbon-budget/2020	(Schwinger et al., 2016)	
	MOM6-COBALT (Princeton)	Global ocean biogeochemistry model output	Global_Carbon_Budget_2020v1.0.xlsx		(Friedlingstein et al., 2020)	https://www.icos-cp.eu/science-and-impact/global-carbon-budget/2020	(Liao et al., 2020)	
	NEMO-PISCES (IPSL)	Global ocean biogeochemistry model output	Global_Carbon_Budget_2020v1.0.xlsx		(Friedlingstein et al., 2020)	https://www.icos-cp.eu/science-and-impact/global-carbon-budget/2020	(Aumont et al., 2015)	
	MPI_SOMFFN	Observation-based data product	ipcc_socom_flux_annual_20191206.csv				(Landschützer et al., 2014)	
	JENA_MLS	Observation-based data product	ipcc_socom_flux_annual_20191206.csv				(Rödenbeck et al., 2014)	
	LSCE_FFNN2	Observation-based data product	ipcc_socom_flux_annual_20191206.csv				(Denvil-Sommer et al., 2019)	
	CSIR_ML6	Observation-based data product	ipcc_socom_flux_annual_20191206.csv				(Gregor et al., 2019)	
	NIES_NN	Observation-based data	ipcc_socom_flux_annual_201912				(Zeng et al., 2014)	

		product	06.csv					
	JMA_MLR	Observation-based data product	ipcc_socom_flux_annual_20191206.csv				(Iida et al., 2020)	
	MIROC4-lr2020	Data of atmospheric CO2 inversion					(Saeki and Patra, 2017)	
	MIROC4-gcp2020	Data of atmospheric CO2 inversion					(Saeki and Patra, 2017)	
	CAMS2020	Data of atmospheric CO2 inversion					(Chevallier et al., 2005)	
	CTE2020	Data of atmospheric CO2 inversion					(van der Laan-Luijkx et al., 2017)	
	The oceanic sink for anthropogenic CO2 from 1994 to 2007 - the data (NCEI Accession 0186034)	Observation-based data product	inv_dcant_emlr_cstar_gruber_94-07_vs1.nc		(Gruber et al., 2019b)	https://www.ncei.noaa.gov/access/ocean-carbon-data-system/oceans/ndp_100/ndp100.html	(Gruber et al., 2019b)	
	Global decadal variability of the oceanic CO2 sink.	Data of global ocean inverse model			(DeVries et al., 2017)		(DeVries et al., 2017)	
	Global carbon budget based on trends in dAPO from three stations in the Scripps O2 network,	Data of global carbon budget from atmospheric O2/N2 and CO2 measurements			(Keeling and Manning, 2014)		(Keeling and Manning, 2014)	
	Global carbon budgets estimated from APO variations in the western	Data of global carbon budget from atmospheric O2/N2 and CO2			(Tohjima et al., 2019)		(Tohjima et al., 2019)	

	Pacific region	measurements						
Figure 5.9 (a)	pCO2 observation-based sea-air CO2 flux products	sea-air CO2 exchange	FCO2DatProd_mean.nc		Fay and Gregor sysnthesis	sea-air CO2 flux synthesis	(Landschützer et al., 2014; Rödenbeck et al., 2014; Zeng et al., 2014; Bakker et al., 2016; Denvil-Sommer et al., 2019; Gregor et al., 2019; Iida et al., 2020)	
Figure 5.9 (b)	Anthropogenic CO2 inventory	Ocean CO2	inv_dcant_emlr_cstar_gruber_94-07_vs1.nc				(Gruber et al., 2019b)	
Figure 5.10 (a)	Global net land CO2 sink	Data derived from global carbon budget	Global_Carbon_Budget_2020v1.0.xlsx		(Friedlingstein et al., 2020)		(Friedlingstein et al., 2020)	
	CarbonTracker-Europe	atmospheric CO2 inversion			(van der Laan-Luijkx et al., 2017)		(van der Laan-Luijkx et al., 2017)	
	Jena CarboScope	atmospheric CO2 inversion			(Rödenbeck et al., 2018)		(Rödenbeck et al., 2018)	
	Copernicus Atmosphere Monitoring Service (CAMS)	atmospheric CO2 inversion			(Chevallier et al., 2005)		(Chevallier et al., 2005)	
	MIROC4-ACTM	atmospheric CO2 inversion			(Patra et al., 2018)		(Patra et al., 2018)	
Figure 5.10 (b)	AVHRR NDVI	satellite data			(Tucker et al., 2005)		(Tucker et al., 2005)	
	MODIS NDVI	satellite data			Didan et al., 2015		Didan, K.. MOD13C2 MODIS/Terra Vegetation Indices Monthly L3 Global 0.05Deg CMG V006. 2015, distributed by	10.5067/MODIS/MOD13C2.006

							NASA EOSDIS Land Processes DAAC	
Figure 5.10 (c)	NIRv	satellite data			(Badgley et al., 2017)		(Badgley et al., 2017)	
	CSIF	satellite data			(Zhang et al., 2018b)		(Zhang et al., 2018b)	
Figure 5.10 (d)	WEC GPP	data-driven GPP product			(Cheng et al., 2017)		(Cheng et al., 2017)	
	MODIS GPP	satellite-based GPP product			Running et al., 2019		Running, S., M. Zhao. MOD17A3HGF MODIS/Terra Net Primary Production Gap-Filled Yearly L4 Global 500 m SIN Grid V006. 2019, distributed by NASA EOSDIS Land Processes DAAC	10.5067/MODIS/MOD17A3HGF.006
Figure 5.11	CarbonTracker-Europe	atmospheric CO2 inversion			van der Laan-Luijkx et al., 2017		(van der Laan-Luijkx et al., 2017)	
	Jena CarboScope	atmospheric CO2 inversion			Rödenbeck et al., 2018		(Rödenbeck et al., 2018)	
	Copernicus Atmosphere Monitoring Service (CAMS)	atmospheric CO2 inversion			Chevallier et al., 2005		(Chevallier et al., 2005)	
	MIROC4-ACTM	atmospheric CO2 inversion			Patra et al., 2018		(Patra et al., 2018)	
	Nino 3.4 index	sea surface temperature reanalysis			(Rayner, 2003)		(Rayner, 2003)	
	CRU	gridded temperature			(Harris et al., 2014)		(Harris et al., 2014)	

		observation						
Figure 5.13 (a)	CH4, Global	NOAA: Global			NOAA		(Dlugokencky et al., 2003)	
	CH4, Global	AGAGE: Global			AGAGE		(Prinn et al., 2018)	
	XCH4, GOSAT	NIES: GOSAT; total column dry air mole fractions	whole-atmosphere-monthly-mean_ch4_january_2021.txt		NIES	NIES, https://www.gosat.nies.go.jp/en/recent-global-ch4.html	(Yoshida et al., 2013)	
	CH4, CMO-THD	PDX: CMO-THD			Portland State University	PDX	(Rice et al., 2016)	
	CH4, CGO	AGAGE: CGO					(Prinn et al., 2018)	
Figure 5.13 (b)	CH4, Global CH4, Global XCH4, GOSAT CH4, CMO-THD CH4, CGO				Chapter 5, AR6		Python 3.8, (Nakazawa et al., 1997) for growth rate calculation	
Figure 5.13 (c)	d13C-CH4, NOAA				NOAA	ftp://aftp.cmdl.noaa.gov/data/trace_gases/ch4c13/flask/	White, J.W.C., B.H. Vaughn, and S.E. Michel (2018), University of Colorado, Institute of Arctic and Alpine Research (INSTAAR), Stable Isotopic Composition of Atmospheric Methane (13C) from the NOAA ESRL Carbon	

							Cycle Cooperative Global Air Sampling Network, 1998-2017, Version: 2018-09-24.	
	d13C-CH4, PDX	PDX: CMO-THD			Portland State University	PDX	(Rice et al., 2016)	
Cross-Chapter Box 5.1 Figure 1	CH4, sources/sinks	GCP-CH4			GCP-CH4		(Kirschke et al., 2013)	
	CH4, sources/sinks	GCP-CH4	WG1 AR6, Table 5.2		GCP-CH4		(Saunois et al., 2020)	
	CH4, concentration	NOAA: Global			NOAA		(Dlugokencky et al., 2003)	
Cross-Chapter Box 5.1 Figure 2	LMDz	CH4 inversion			GCP-CH4		(Bousquet et al., 2006)	
	TM5-4DVAR	CH4 inversion			GCP-CH4		(Bergamaschi et al., 2013)	
	CTE-CH4	CH4 inversion			GCP-CH4		(Tsuruta et al., 2017)	
	MIROC4-ACTM	CH4 inversion			GCP-CH4		(Chandra et al., 2021)	
	LMDzPyVAR	CH4 inversion			GCP-CH4		(Yin et al., 2015)	
	NICAM-TM	CH4 inversion			GCP-CH4		(Niwa et al., 2017)	
	NIES-TM-Flexpart	CH4 inversion			GCP-CH4		(Wang et al., 2019a)	
	NIES-TM-GELCA	CH4 inversion			GCP-CH4		(Ishizawa et al., 2016)	
	TOMCAT	CH4 inversion			GCP-CH4		(McNorton et al., 2018)	
	GCP-WETLAND mean	Land ecosystem model			GCP-CH4		(Saunois et al., 2020)	
Figure 5.15 (a)	NOAA atmospheric N2O network	input dataset	n2o_gbl_mean_grate_noaa.txt			https://www.esrl.noaa.gov/gmd/dv/data/	Elkins, J. W., Dlugokencky, E., Hall, B., Dutton,	https://www.esrl.noaa.gov/gmd/hats/combined/N2

	dataset						G., Nance, D., and Mondeel, D. J. (2018). Combined Nitrous Oxide data from the NOAA/ESRL Global Monitoring Division. Earth Syst. Res. Lab. (ESRL), Natl. Ocean. Atmos. Adm. Available at: https://www.esrl.noaa.gov/gmd/hats/combined/N2O.html [Accessed January 24, 2019].	O.html
	AGAGE atmospheric N2O network dataset	input dataset	n2o_gbl_mean_grate_agage.txt			https://agage2.eas.gatech.edu/data_archive/agage/	(Prinn et al., 2018)	
	CSIRO atmospheric N2O network dataset	input dataset	n2o_gbl_mean_grate_csiro.txt			https://gaw.kishou.go.jp/	(Francey et al., 2003) Available at: http://hdl.handle.net/102.100.100/194315?index=1.	
	Archived air sampes from Cape Grim	input dataset	N2O_isotope_CGAA_Park_2012.csv				(Park et al., 2012)	
	firn air data set Law Dome	input dataset	N2O_isotope_LD_Park_2012.csv				(Park et al., 2012)	
	firn air data set	input dataset	N2O_isotope_N			https://ads.nipr.a	(Ishijima et al.,	

	NGRIP		GRIP_Ishijima_2007.csv			c.jp/data/search/list/1	2007)	
	firn air data set H72	input dataset	N2O_isotope_H72_Ishijima_2007.csv			https://ads.nipr.ac.jp/data/search/list/1	(Ishijima et al., 2007)	
	firn ice data set Greenland	input dataset	N2O_isotope_BRK_Prokopiou.csv				(Prokopiou et al., 2017)	
	firn ice data set Greenland	input dataset	N2O_isotope_DC_Prokopiou.csv				(Prokopiou et al., 2017)	
	firn ice data set Greenland	input dataset	N2O_isotope_DML_Prokopiou.csv				(Prokopiou et al., 2017)	
	firn ice data set Greenland	input dataset	N2O_isotope_NGR_SB_Prokopiou.csv				(Prokopiou et al., 2017)	
	firn ice data set Greenland	input dataset	N2O_isotope_NEEM_09_Prokopiou.csv				(Prokopiou et al., 2017)	
	firn ice data set Greenland	input dataset	N2O_isotope_NEEM_EU_Prokopiou.csv				(Prokopiou et al., 2017)	
	Multivariate Enso Index	input dataset	noaa_mei_index_1979_2020.txt			https://psl.noaa.gov/enso/mei	(Wolter and Timlin, 1998)	
Figure 5.15 (b)	Archived air sampes from Cape Grim	input dataset	N2O_isotope_CGAA_Park_2012.csv				(Park et al., 2012)	
	firn air data set Law Dome	input dataset	N2O_isotope_LD_Park_2012.csv				(Park et al., 2012)	
	firn air data set NGRIP	input dataset	N2O_isotope_NGRIP_Ishijima_2007.csv				(Ishijima et al., 2007)	
	firn air data set H72	input dataset	N2O_isotope_H72_Ishijima_2007.csv				(Ishijima et al., 2007)	
	firn ice data set Greenland	input dataset	N2O_isotope_BRK_Prokopiou.c				(Prokopiou et al., 2017)	

			sv					
	firn ice data set Greenland	input dataset	N2O_isotope_DC_Prokopiou.csv				(Prokopiou et al., 2017)	
	firn ice data set Greenland	input dataset	N2O_isotope_DML_Prokopiou.csv				(Prokopiou et al., 2017)	
	firn ice data set Greenland	input dataset	N2O_isotope_NGR_SB_Prokopiou.csv				(Prokopiou et al., 2017)	
	firn ice data set Greenland	input dataset	N2O_isotope_NEEM_09_Prokopiou.csv				(Prokopiou et al., 2017)	
	firn ice data set Greenland	input dataset	N2O_isotope_NEEM_EU_Prokopiou.csv				(Prokopiou et al., 2017)	
Figure 5.15 (c)	Archived air sampes from Cape Grim	input dataset	N2O_isotope_CGAA_Park_2012.csv				(Park et al., 2012)	
	firn air data set H72	input dataset	N2O_isotope_H72_Ishijima_2007.csv				(Ishijima et al., 2007)	
	firn ice data set Greenland	input dataset	N2O_isotope_BRK_Prokopiou.csv				(Prokopiou et al., 2017)	
	firn ice data set Greenland	input dataset	N2O_isotope_DC_Prokopiou.csv				(Prokopiou et al., 2017)	
	firn ice data set Greenland	input dataset	N2O_isotope_DML_Prokopiou.csv				(Prokopiou et al., 2017)	
	firn ice data set Greenland	input dataset	N2O_isotope_NGR_SB_Prokopiou.csv				(Prokopiou et al., 2017)	
	firn ice data set Greenland	input dataset	N2O_isotope_NEEM_09_Prokopiou.csv				(Prokopiou et al., 2017)	
	firn ice data set Greenland	input dataset	N2O_isotope_NEEM_EU_Prokopiou.csv				(Prokopiou et al., 2017)	
Figure 5.17 (a)	land mean N2O	model simulation	N2O_emission_d	IPCC data	GCP-N2O-		(Tian et al.,	

	flux (2007-2016 average)		ensity_IPCC_0716.txt	agreement available	budget		2020)	
	baseline mean & range	model simulation	ocean_mean_0716.txt	IPCC data agreement available	GCP-N2O-budget		(Tian et al., 2020)	
Figure 5.17 (b-p)	total mean & range	model simulation	IPCC_NMPI_all_forcing.xlsx	IPCC data agreement available	NMIP		(Tian et al., 2019)	
	baseline mean & range	model simulation	IPCC_NMPI_co2_climate.xlsx	IPCC data agreement available	NMIP		(Tian et al., 2019)	
Figure 5.18	Effective Radiative Forcing	input dataset	AR6_ERF_all.xlsx		Chapter 7, AR6		Forster, P., et al., Chapter 7, AR6, 2021	
Figure 5.19	CarbonTracker-Europe	CO2 inversion			GCP-CO2		(van der Laan-Luijkx et al., 2017)	contact: wouter.peters@wur.nl, ingrid.luijkx@wur.nl
	Jena Carboscope	CO2 inversion			GCP-CO2		(Rödenbeck et al., 2018)	contact: Christian.Roedenbeck@bgc-jena.mpg.de
	CAMS	CO2 inversion			GCP-CO2		(Chevallier et al., 2005)	contact: frederic.chevallier@lsce.ipsl.fr
	MIROC4-ACTM	CO2 inversion			GCP-CO2		(Patra et al., 2018)	contact: prabir@jamstec.go.jp, naveennegi@jamstec.go.jp
	NISMON-CO2	CO2 inversion			GCP-CO2		(Niwa et al., 2017)	contact: niwa.yosuke@nies.go.jp
	LMDz	CH4 inversion			GCP-CH4		(Bousquet et al., 2006)	
	TM5-4DVAR	CH4 inversion			GCP-CH4		(Bergamaschi et al., 2013)	
	CTE-CH4	CH4 inversion			GCP-CH4		(Tsuruta et al., 2017)	

	MIROC4-ACTM	CH4 inversion			GCP-CH4		(Chandra et al., 2021)	
	LMDzPyVAR	CH4 inversion			GCP-CH4		(Yin et al., 2015)	
	NICAM-TM	CH4 inversion			GCP-CH4		(Niwa et al., 2017)	
	NIES-TM-Flexpart	CH4 inversion			GCP-CH4		(Wang et al., 2019a)	
	NIES-TM-GELCA	CH4 inversion			GCP-CH4		(Ishizawa et al., 2016)	
	TOMCAT	CH4 inversion			GCP-CH4		(McNorton et al., 2018)	
	INVICAT	N2O inversion			GCP-N2O		(Thompson et al., 2019)	C.Wilson@leeds.ac.uk (Chris Wilson)
	PyVAR-1	N2O inversion			GCP-N2O		rlt@nilu.no (Rona Thompson)	
	PyVAR-2	N2O inversion			GCP-N2O		rlt@nilu.no (Rona Thompson)	
	MIRO4-ACTM	N2O inversion			GCP-N2O		prabir@jamstec.go.jp (Prabir Patra)	
	GEOS-Chem	N2O inversion			GCP-N2O		(Tian et al., 2020)	kcw@umn.edu (Kelly Wells)
Figure 5.20	Global surface ocean pH, acidity, and Revelle Factor on a 1x1 degree global grid from 1770 to 2100 (NCEI Accession 0206289)	observation-based dataset	Surface_pH_1770_2000.nc		(Jiang et al., 2019)	https://www.ncei.noaa.gov/data/oceans/ncei/ocads/data/0206289/Surface_pH_1770_2100	(Jiang et al., 2019)	
	Annual mean seasonally-detrended surface ocean pH	observation-based dataset	annual_mean_pH_seosonally_detrended.xlsx					

	at time-series sites							
	Time-series data of surface ocean pH at 137E	observation-based dataset	137E_surface_carbon.xlsx			https://www.data.jma.go.jp/gmd/kaiyou/db/vessel_obs/data-report/html/ship/ship_e	(Ono et al., 2019)	
	Time-series data of surface ocean pH at stations KNOT and K2	observation-based dataset	KNOT_ML.csv, K2_ML.csv			https://www.ncei.noaa.gov/access/ocean-carbon-data-system/oceans/Moorings/K2.html	(Wakita et al., 2017)	
	Time-series data of surface ocean pH at station ALOHA	observation-based dataset	HOT_surface_CO2.txt		(Dore et al., 2009b)	https://hahana.soest.hawaii.edu/hot/products/HOT_surface_CO2.txt	(Dore et al., 2009b)	
	Time-series data of surface ocean pH at the BATS site	observation-based dataset	43247_2020_30_MOESM2_ESM.xlsx		(Bates and Johnson, 2020)	https://www.nature.com/articles/s43247-020-00030-5#Sec22	(Bates and Johnson, 2020)	
	Time-series data of surface ocean pH in the Iceland Sea	observation-based dataset	IcelandSea.exc.csv, IcelandSea_LN6_2014-2019.csv			https://www.ncei.noaa.gov/access/ocean-carbon-data-system/oceans/Moorings/Iceland_Sea.html	(Olafsson et al., 2009)	
	Time-series data of surface ocean pH at the DYFAMED site	observation-based dataset	DYFAMED_surface_pH.csv			https://www.ncei.noaa.gov/access/ocean-carbon-data-system/oceans/Coastal/DYFAMED.html	(Merlivat et al., 2018)	
	Time-series data of surface ocean pH at the ESTOC site	observation-based dataset	ESTOC_TS_Data_1995-2016.csv			https://www.ncei.noaa.gov/access/ocean-carbon-data-	(González-Dávila et al., 2010)	

						system/oceans/Coastal/ESTOC.html		
	Time-series data of surface ocean pH at the CARIACO site	observation-based dataset	CARIACO_surface_pH.csv			http://imars.marine.usf.edu/CAR-legacy/Master.txt	(Bates et al., 2014)	
	Time-series data of surface ocean pH at the Drake Passage	observation-based dataset	DrakePass_pH_Omega_LDEO_030519.PRT.xlsx		(Takahashi et al., 2014)	https://www.ldeo.columbia.edu/res/pi/CO2/carbondioxide/pages/pCO2data.html	(Takahashi et al., 2014)	
	Time-series data of surface ocean pH at the Munida site	observation-based dataset	MunidaTimeSeries210106.csv			https://marinedata.niwa.co.nz/nzoa-on-map/	(Bates et al., 2014)	
Figure 5.21	GLODAPv2 Mapped Data Product	observation-based dataset	GLODAPv2.2016b_MappedClimatologies.tar.gz		(Lauvset et al., 2016)	https://www.glodap.info/index.php/mapped-data-product/	(Lauvset et al., 2020)	
					(Olsen et al., 2016)	https://doi.org/10.5194/essd-8-297-2016		
Figure 5.31	IPCC AR6 assessed historical GSAT time series (Chapter 2)							
	Global Carbon Budget 2020	Input Dataset	2020_Global_Budget_v1.0.xlsx			10.18160/gcp-2020	(Friedlingstein et al., 2020)	
FAQ 5.1	Global Carbon Budget 2020	Input Dataset	2020_Global_Budget_v1.0.xlsx			10.18160/gcp-2020	(Friedlingstein et al., 2020)	
FAQ 5.2	Northern Circumpolar Soil Carbon Database version 2 (NCSCDv2)	Input Dataset			(Hugelius et al., 2013)	https://bolin.su.se/data/ncscd/		
	Circumpolar Thermokarst Landscapes	Input Dataset			(Olefeldt et al., 2016)			

	Database							

[END TABLE 5.SM.6 HERE]

References

Atlas, R., Hoffman, R. N., Ardizzone, J., Leidner, S. M., Jusem, J. C., Smith, D. K., et al. (2011). A Cross-calibrated, Multiplatform Ocean Surface Wind Velocity Product for Meteorological and Oceanographic Applications. *Bull. Am. Meteorol. Soc.* 92, 157–174. doi:10.1175/2010BAMS2946.1.

Aumont, O., Ethé, C., Tagliabue, A., Bopp, L., and Gehlen, M. (2015). PISCES-v2: an ocean biogeochemical model for carbon and ecosystem studies. *Geosci. Model Dev.* 8, 2465–2513. doi:10.5194/gmd-8-2465-2015.

Badgley, G., Field, C. B., and Berry, J. A. (2017). Canopy near-infrared reflectance and terrestrial photosynthesis. *Sci. Adv.* 3. doi:10.1126/sciadv.1602244.

Bakker, D. C. E., Pfeil, B., Landa, C. S., Metzl, N., O'Brien, K. M., Olsen, A., et al. (2016). A multi-decade record of high-quality fCO2 data in version 3 of the Surface Ocean CO2 Atlas (SOCAT). *Earth Syst. Sci. Data* 8, 383–413. doi:10.5194/essd-8-383-2016.

Bates, N., Astor, Y., Church, M., Currie, K., Dore, J., Gonaález-Dávila, M., et al. (2014). A Time-Series View of Changing Ocean Chemistry Due to Ocean Uptake of Anthropogenic CO2 and Ocean Acidification. *Oceanography* 27, 126–141. doi:10.5670/oceanog.2014.16.

Bates, N. R., and Johnson, R. J. (2020). Acceleration of ocean warming, salinification, deoxygenation and acidification in the surface subtropical North Atlantic Ocean. *Commun. Earth Environ.* 1, 33. doi:10.1038/s43247-020-00030-5.

Battle, M., Bender, M. L., Tans, P. P., White, J. W. C., Ellis, J. T., Conway, T., et al. (2000). Global Carbon Sinks and Their Variability Inferred from Atmospheric O₂ and δ¹³C. *Science (80-.).* 287, 2467. doi:10.1126/science.287.5462.2467.

Bauman, S., Costa, M., Fong, M., House, B., Perez, E., Tan, M., et al. (2014). Augmenting the Biological Pump: The Shortcomings of Geoengineered Upwelling. *Oceanography* 27, 17–23. doi:10.5670/oceanog.2014.79.

Beerling, D. J., Leake, J. R., Long, S. P., Scholes, J. D., Ton, J., Nelson, P. N., et al. (2018). Farming with crops and rocks to address global climate, food and soil security. *Nat. Plants* 4, 138–147. doi:10.1038/s41477-018-0108-y.

Benanti, G., Saunders, M., Tobin, B., and Osborne, B. (2014). Contrasting impacts of afforestation on nitrous oxide and methane emissions. *Agric. For. Meteorol.* 198–199, 82–93. doi:10.1016/j.agrformet.2014.07.014.

Bender, M. L., Ho, D. T., Hendricks, M. B., Mika, R., Battle, M. O., Tans, P. P., et al. (2005). Atmospheric O2/N2 changes, 1993–2002: Implications for the partitioning of fossil fuel CO2 sequestration. *Global Biogeochem. Cycles* 19. doi:https://doi.org/10.1029/2004GB002410.

Bereiter, B., Eggleston, S., Schmitt, J., Nehrbass-Ahles, C., Stocker, T. F., Fischer, H., et al. (2015). Revision of the EPICA Dome C CO2 record from 800 to 600-kyr before present. *Geophys. Res. Lett.* 42, 542–549. doi:10.1002/2014GL061957.

Bergamaschi, P., Houweling, S., Segers, A., Krol, M., Frankenberg, C., Scheepmaker, R. A., et al. (2013). Atmospheric CH 4 in the first decade of the 21st century: Inverse modeling analysis using SCIAMACHY satellite retrievals and NOAA surface measurements. *J. Geophys. Res. Atmos.* 118, 7350–7369. doi:10.1002/jgrd.50480.

Berthet, S., Séférian, R., Bricaud, C., Chevallier, M., Voldoire, A., and Ethé, C. (2019). Evaluation of an Online Grid-Coarsening Algorithm in a Global Eddy-Admitting Ocean Biogeochemical Model. *J. Adv. Model. Earth Syst.* 11, 1759–1783. doi:10.1029/2019MS001644.

Bindoff, N. L., Cheung, W. W. L., Kairo, J. G., Arístegui, J., Guinder, V. A., Hallberg, R., et al. (2019). "Changing Ocean, Marine Ecosystems, and Dependent Communities," in *IPCC Special Report on the Ocean and Cryosphere in a Changing Climate*, eds. H.-O. Pörtner, D. C. Roberts, V. Masson-Delmotte, P. Zhai, M. Tignor, E. Poloczanska, et al. (In Press), 447–588. Available at: https://www.ipcc.ch/srocc/chapter/chapter-5.

Blanc-Betes, E., Kantola, I. B., Gomez-Casanovas, N., Hartman, M. D., Parton, W. J., Lewis, A. L., et al. In silico assessment of the potential of basalt amendments to reduce N2O emissions from bioenergy crops. *GCB Bioenergy* n/a. doi:10.1111/gcbb.12757.

Bock, M., Schmitt, J., Beck, J., Seth, B., Chappellaz, J., and Fischer, H. (2017). Glacial/interglacial wetland, biomass burning, and geologic methane emissions constrained by dual stable isotopic CH 4 ice core records. *Proc. Natl. Acad. Sci.* 114, E5778–E5786. doi:10.1073/pnas.1613883114.

Bousquet, P., Ciais, P., Miller, J. B., Dlugokencky, E. J., Hauglustaine, D. A., Prigent, C., et al. (2006). Contribution of anthropogenic and natural sources to atmospheric methane variability. *Nature* 443, 439–443. doi:10.1038/nature05132.

Boyd, P. W., Jickells, T., Law, C. S., Blain, S., Boyle, E. A., Buesseler, K. O., et al. (2007). Mesoscale Iron Enrichment Experiments 1993-2005: Synthesis and Future Directions. *Science (80-.).* 315, 612–617. doi:10.1126/science.1131669.

Boysen, L. R., Lucht, W., and Gerten, D. (2017). Trade-offs for food production, nature conservation and climate limit the terrestrial carbon dioxide removal potential. *Glob. Chang. Biol.* 23, 4303–4317. doi:10.1111/gcb.13745.

Buitenhuis, E. T., Hashioka, T., and Quéré, C. Le (2013). Combined constraints on global ocean primary production using observations and models. *Global Biogeochem. Cycles* 27, 847–858. doi:10.1002/gbc.20074.

Buss, W., and Mašek, O. (2016). High-VOC biochar—effectiveness of post-treatment measures and potential health risks related to handling and storage. *Environ. Sci. Pollut. Res.* 23, 19580–19589. doi:10.1007/s11356-016-7112-4.

Butterworth, B. J., and Miller, S. D. (2016). Air-sea exchange of carbon dioxide in the Southern Ocean and Antarctic marginal ice zone. *Geophys. Res. Lett.* 43, 7223–7230. doi:10.1002/2016GL069581.

Cao, L., and Caldeira, K. (2010). Can ocean iron fertilization mitigate ocean acidification? *Clim. Change* 99, 303–311. doi:10.1007/s10584-010-9799-4.

Cayuela, M. L., van Zwieten, L., Singh, B. P., Jeffery, S., Roig, A., and Sánchez-Monedero, M. A. (2014). Biochar's role in mitigating soil nitrous oxide emissions: A review and meta-analysis. *Agric. Ecosyst. Environ.* 191, 5–16. doi:10.1016/j.agee.2013.10.009.

Chandra, N., Patra, P. K., Bisht, J. S. H., Ito, A., Umezawa, T., Saigusa, N., et al. (2021). Emissions from the Oil and Gas Sectors, Coal Mining and Ruminant Farming Drive Methane Growth over the Past Three Decades. *J. Meteorol. Soc. Japan. Ser. II* 99. doi:10.2151/jmsj.2021-015.

Chaudhuri, A. H., Ponte, R. M., and Nguyen, A. T. (2014). A Comparison of Atmospheric Reanalysis Products for the Arctic Ocean and Implications for Uncertainties in Air–Sea Fluxes. *J. Clim.* 27, 5411–5421. doi:10.1175/JCLI-D-13-00424.1.

Chen, P., Zhou, M., Wang, S., Luo, W., Peng, T., Zhu, B., et al. (2019). Effects of afforestation on soil CH4 and N2O fluxes in a subtropical karst landscape. *Sci. Total Environ.*, 135974. doi:https://doi.org/10.1016/j.scitotenv.2019.135974.

Cheng, L., Zhang, L., Wang, Y.-P., Canadell, J. G., Chiew, F. H. S., Beringer, J., et al. (2017). Recent increases in terrestrial carbon uptake at little cost to the water cycle. *Nat. Commun.* 8, 110. doi:10.1038/s41467-017-00114-5.

Chevallier, F. (2013). On the parallelization of atmospheric inversions of CO2 surface fluxes within a variational framework. *Geosci. Model Dev.* 6, 783–790. doi:10.5194/gmd-6-783-2013.

Chevallier, F., Fisher, M., Peylin, P., Serrar, S., Bousquet, P., Bréon, F.-M., et al. (2005). Inferring CO2 sources and sinks from satellite observations: Method and application to TOVS data. *J. Geophys. Res.* 110, D24309. doi:10.1029/2005JD006390.

Ciais, P., Sabine, C., Bala, G., Bopp, L., Brovkin, V., Canadell, J., et al. (2013). "Carbon and Other Biogeochemical Cycles," in *Climate Change 2013: The Physical Science Basis. Contribution of Working Group I to the Fifth Assessment Report of the Intergovernmental Panel on Climate Change*, eds. T. F. Stocker, D. Qin, G.-K. Plattner, M. Tignor, S. K. Allen, J. Boschung, et al. (Cambridge, United Kingdom and New York, NY, USA: Cambridge University Press), 465–570. doi:10.1017/CBO9781107415324.015.

Claustre, H., Johnson, K. S., and Takeshita, Y. (2020). Observing the global ccean with biogeochemical-argo. *Ann. Rev. Mar. Sci.* 12. doi:10.1146/annurev-marine-010419-010956.

Clement, D., and Gruber, N. (2018). The eMLR(C*) method to determine decadal changes in the global ocean storage of anthropogenic CO2. *Global Biogeochem. Cycles* 32, 654–679. doi:10.1002/2017GB005819.

Clough, T., Condron, L., Kammann, C., and Müller, C. (2013). A review of biochar and soil nitrogen dynamics. *Agronomy* 3, 275–293. doi:10.3390/agronomy3020275.

Conway, T. J., Tans, P. P., Waterman, L. S., Thoning, K. W., Kitzis, D. R., Masarie, K. A., et al. (1994). Evidence for interannual variability of the carbon cycle from the National Oceanic and Atmospheric Administration/Climate Monitoring and Diagnostics Laboratory Global Air Sampling Network. *J. Geophys. Res.* 99, 22831. doi:10.1029/94JD01951.

Creutzig, F., Breyer, C., Hilaire, J., Minx, J., Peters, G. P., and Socolow, R. (2019). The mutual dependence of negative emission technologies and energy systems. *Energy Environ. Sci.* 12, 1805–1817. doi:10.1039/C8EE03682A.

Creutzig, F., Ravindranath, N. H., Berndes, G., Bolwig, S., Bright, R., Cherubini, F., et al. (2015). Bioenergy and climate change mitigation: an assessment. *GCB Bioenergy* 7, 916–944. doi:10.1111/gcbb.12205.

Daneshvar, F., Nejadhashemi, A. P., Adhikari, U., Elahi, B., Abouali, M., Herman, M. R., et al. (2017). Evaluating the significance of wetland restoration scenarios on phosphorus removal. *J. Environ. Manage.* 192, 184–196. doi:10.1016/j.jenvman.2017.01.059.

Davin, E. L., Seneviratne, S. I., Ciais, P., Olioso, A., and Wang, T. (2014). Preferential cooling of hot extremes from cropland albedo management. *Proc. Natl. Acad. Sci.* 111, 9757–9761. doi:10.1073/pnas.1317323111.

Deng, N., Wang, H., Hu, S., and Jiao, J. (2019). Effects of Afforestation Restoration on Soil Potential N2O Emission and Denitrifying Bacteria After Farmland Abandonment in the Chinese Loess Plateau. *Front. Microbiol.* 10, 262. doi:10.3389/fmicb.2019.00262.

Denman, K. L., Brasseur, G. P., Chidthaisong, A., Ciais, P., Cox, P. M., Dickinson, R. E., et al. (2007). "Couplings Between Changes in the Climate System and Biogeochemistry," in *Climate Change 2007: The Physical Science Basis. Contribution of Working Group I to the Fourth Assessment Report of the Intergovernmental Panel on Climate*

Change, eds. S. Solomon, D. Qin, M. Manning, Z. Chen, M. Marquis, K. B. Averyt, et al. (Cambridge, United Kingdom and New York, NY, USA: Cambridge University Press), 499–588. Available at: https://www.ipcc.ch/report/ar4/wg1.

Denvil-Sommer, A., Gehlen, M., Vrac, M., and Mejia, C. (2019). LSCE-FFNN-v1: a two-step neural network model for the reconstruction of surface ocean pCO2 over the global ocean. *Geosci. Model Dev.* 12, 2091–2105. doi:10.5194/gmd-12-2091-2019.

Devaraju, N., Bala, G., and Modak, A. (2015a). Effects of large-scale deforestation on precipitation in the monsoon regions: Remote versus local effects. *Proc. Natl. Acad. Sci.* 112, 3257–3262. doi:10.1073/pnas.1423439112.

Devaraju, N., Bala, G., and Nemani, R. (2015b). Modelling the influence of land-use changes on biophysical and biochemical interactions at regional and global scales. *Plant. Cell Environ.* 38, 1931–1946. doi:10.1111/pce.12488.

DeVries, T., Holzer, M., and Primeau, F. (2017). Recent increase in oceanic carbon uptake driven by weaker upper-ocean overturning. *Nature* 542, 215–218. doi:10.1038/nature21068.

Dlugokencky, E. J., Houwelling, S., Bruhwiler, L., Masarie, K. A., Lang, P. M., Miller, J. B., et al. (2003). Atmospheric methane levels off: Temporary pause or a new steady-state? *Geophys. Res. Lett.* 30, 1992. doi:10.1029/2003GL018126.

Dlugokencky, E., and Tans, P. . (2020). Trends in atmospheric carbon dioxide, National Oceanic and Atmospheric Administration. *Earth Syst. Res. Lab.*

Don, A., Osborne, B., Hastings, A., Skiba, U., Carter, M. S., Drewer, J., et al. (2012). Land-use change to bioenergy production in Europe: implications for the greenhouse gas balance and soil carbon. *GCB Bioenergy* 4, 372–391. doi:10.1111/j.1757-1707.2011.01116.x.

Doney, S. C., Lima, I., Feely, R. A., Glover, D. M., Lindsay, K., Mahowald, N., et al. (2009a). Mechanisms governing interannual variability in upper-ocean inorganic carbon system and air–sea CO2 fluxes: Physical climate and atmospheric dust. *Deep Sea Res. Part II Top. Stud. Oceanogr.* 56, 640–655. doi:10.1016/j.dsr2.2008.12.006.

Doney, S. C., Lima, I., Feely, R. A., Glover, D. M., Lindsay, K., Mahowald, N., et al. (2009b). Mechanisms governing interannual variability in upper-ocean inorganic carbon system and air–sea CO2 fluxes: Physical climate and atmospheric dust. *Deep Sea Res. Part II Top. Stud. Oceanogr.* 56, 640–655. doi:https://doi.org/10.1016/j.dsr2.2008.12.006.

Dore, J. E., Lukas, R., Sadler, D. W., Church, M. J., and Karl, D. M. (2009a). Physical and biogeochemical modulation of ocean acidification in the central North Pacific. *Proc. Natl. Acad. Sci.* 106, 12235–12240. doi:10.1073/PNAS.0906044106.

Dore, J. E., Lukas, R., Sadler, D. W., Church, M. J., and Karl, D. M. (2009b). Physical and biogeochemical modulation of ocean acidification in the central North Pacific. *Proc. Natl. Acad. Sci.* 106, 12235–12240. doi:10.1073/pnas.0906044106.

Fairaill, C. W., Hare, J. E., Edson, J. B., and McGillis, W. (2000). Parameterization and Micrometeorological Measurement of Air–Sea Gas Transfer. *Boundary-Layer Meteorol.* 96, 63–106. doi:10.1023/A:1002662826020.

Farley, K. A., Jobbagy, E. G., and Jackson, R. B. (2005). Effects of afforestation on water yield: a global synthesis with implications for policy. *Glob. Chang. Biol.* 11, 1565–1576. doi:10.1111/j.1365-2486.2005.01011.x.

Fay, A. R., and McKinley, G. A. (2014). Global open-ocean biomes: mean and temporal variability. *Earth Syst. Sci. Data* 6, 273–284. doi:10.5194/essd-6-273-2014.

Feng, E. Y., Koeve, W., Keller, D. P., and Oschlies, A. (2017). Model-based assessment of the CO2 sequestration potential of coastal ocean alkalinization. *Earth's Futur.* 5, 1252–1266. doi:10.1002/2017EF000659.

Feng, E. Y., Su, B., and Oschlies, A. (2020). Geoengineered Ocean Vertical Water Exchange Can Accelerate Global Deoxygenation. *Geophys. Res. Lett.* 47, e2020GL088263. doi:10.1029/2020GL088263.

Fischer, B. M. C., Manzoni, S., Morillas, L., Garcia, M., Johnson, M. S., and Lyon, S. W. (2019). Improving agricultural water use efficiency with biochar – A synthesis of biochar effects on water storage and fluxes across scales. *Sci. Total Environ.* 657, 853–862. doi:10.1016/j.scitotenv.2018.11.312.

Flecha, S., Pérez, F. F., Murata, A., Makaoui, A., and Huertas, I. E. (2019). Decadal acidification in Atlantic and Mediterranean water masses exchanging at the Strait of Gibraltar. *Sci. Rep.* 9, 15533. doi:10.1038/s41598-019-52084-x.

Fornara, D. A., Steinbeiss, S., McNamara, N. P., Gleixner, G., Oakley, S., Poulton, P. R., et al. (2011). Increases in soil organic carbon sequestration can reduce the global warming potential of long-term liming to permanent grassland. *Glob. Chang. Biol.* 17, 1925–1934. doi:10.1111/j.1365-2486.2010.02328.x.

Foster, G. L., Royer, D. L., and Lunt, D. J. (2017). Future climate forcing potentially without precedent in the last 420 million years. *Nat. Commun.* 8, 14845. doi:10.1038/ncomms14845.

Francey, R. J., Steele, L. P., Spencer, D. A., Langenfelds, R. L., Law, R. M., Krummel, P. B., et al. (2003). "The CSIRO (Australia) measurement of greenhouse gases in the global atmosphere," in WMO TD No. 1138., eds. S. Toru and S.

Kazuto (Geneva, Switzerland: World Meteorological Organization (WMO)), 97–111. Available at: https://library.wmo.int/index.php?lvl=notice_display&id=11080#.YHA_RtV1DIU.
Friedlingstein, P., Jones, M. W., O'Sullivan, M., Andrew, R. M., Hauck, J., Peters, G. P., et al. (2019). Global Carbon Budget 2019. *Earth Syst. Sci. Data* 11, 1783–1838. doi:10.5194/essd-11-1783-2019.
Friedlingstein, P., O'Sullivan, M., Jones, M. W., Andrew, R. M., Hauck, J., Olsen, A., et al. (2020). Global Carbon Budget 2020. *Earth Syst. Sci. Data* 12, 3269–3340. doi:10.5194/essd-12-3269-2020.
Fuss, S., Lamb, W. F., Callaghan, M. W., Hilaire, J., Creutzig, F., Amann, T., et al. (2018). Negative emissions – Part 2: Costs, potentials and side effects. *Environ. Res. Lett.* 13, 063002. doi:10.1088/1748-9326/aabf9f.
Garbe, C. S., Rutgersson, A., Boutin, J., de Leeuw, G., Delille, B., Fairall, C. W., et al. (2014). "Transfer across the air-sea interface," in *Ocean-Atmosphere Interactions of Gases and Particles* (Springer Berlin Heidelberg), 55–112. doi:10.1007/978-3-642-25643-1_2.
Gasser, T., Crepin, L., Quilcaille, Y., Houghton, R. A., Ciais, P., and Obersteiner, M. (2020). Historical CO2 emissions from land use and land cover change and their uncertainty. *Biogeosciences* 17, 4075–4101. doi:10.5194/bg-17-4075-2020.
Genesio, L., Miglietta, F., Lugato, E., Baronti, S., Pieri, M., and Vaccari, F. P. (2012). Surface albedo following biochar application in durum wheat. *Environ. Res. Lett.* 7, 014025. doi:10.1088/1748-9326/7/1/014025.
GESAMP (2019). High level review of a wide range of proposed marine geoengineering techniques.
Gloor, M., Gruber, N., Sarmiento, J., Sabine, C. L., Feely, R. A., and Rödenbeck, C. (2003). A first estimate of present and preindustrial air-sea CO2 flux patterns based on ocean interior carbon measurements and models. *Geophys. Res. Lett.* 30, 10-1-10–4. doi:https://doi.org/10.1029/2002GL015594.
González-Dávila, M., Santana-Casiano, J. M., Rueda, M. J., and Llinás, O. (2010). The water column distribution of carbonate system variables at the ESTOC site from 1995 to 2004. *Biogeosciences* 7, 3067–3081. doi:10.5194/bg-7-3067-2010.
González, M. F., and Ilyina, T. (2016). Impacts of artificial ocean alkalinization on the carbon cycle and climate in Earth system simulations. *Geophys. Res. Lett.* 43, 6493–6502. doi:10.1002/2016GL068576.
González, M. F., Ilyina, T., Sonntag, S., and Schmidt, H. (2018). Enhanced rates of regional warming and ocean acidification after termination of large-scale ocean alkalinization. *Geophys. Res. Lett.* 45, 7120–7129. doi:10.1029/2018GL077847.
Good, S. A., Martin, M. J., and Rayner, N. A. (2013). EN4: Quality controlled ocean temperature and salinity profiles and monthly objective analyses with uncertainty estimates. *J. Geophys. Res. Ocean.* 118, 6704–6716. doi:10.1002/2013JC009067.
Good, S., Fiedler, E., Mao, C., Martin, M. J., Maycock, A., Reid, R., et al. (2020). The Current Configuration of the OSTIA System for Operational Production of Foundation Sea Surface Temperature and Ice Concentration Analyses. *Remote Sens.* 12, 720. doi:10.3390/rs12040720.
Graven, H. D., Gruber, N., Key, R., Khatiwala, S., and Giraud, X. (2012). Changing controls on oceanic radiocarbon: New insights on shallow-to-deep ocean exchange and anthropogenic CO2 uptake. *J. Geophys. Res. Ocean.* 117. doi:https://doi.org/10.1029/2012JC008074.
Gray, A. R., Johnson, K. S., Bushinsky, S. M., Riser, S. C., Russell, J. L., Talley, L. D., et al. (2018). Autonomous biogeochemical Ffoats detect significant carbon dioxide outgassing in the high-latitude Southern Ocean. *Geophys. Res. Lett.* 45, 9049–9057. doi:10.1029/2018GL078013.
Gregor, L., and Fay, A. R. (2021). SeaFlux data set: Air-sea CO2 fluxes for surface pCO2 data products using a standardised approach. Zenodo. *SeaFlux data set Air-sea CO2 fluxes Surf. pCO2 data Prod. using a Stand. approach. Zenodo*. doi:/10.5281/zenodo.4133802, 2021.
Gregor, L., Lebehot, A. D., Kok, S., and Scheel Monteiro, P. M. (2019). A comparative assessment of the uncertainties of global surface ocean CO2 estimates using a machine-learning ensemble (CSIR-ML6 version 2019a) – have we hit the wall? *Geosci. Model Dev.* 12, 5113–5136. doi:10.5194/gmd-12-5113-2019.
Griscom, B. W., Adams, J., Ellis, P. W., Houghton, R. A., Lomax, G., Miteva, D. A., et al. (2017). Natural climate solutions. *Proc. Natl. Acad. Sci.* 114, 11645–11650. doi:10.1073/pnas.1710465114.
Gruber, N., Clement, D., Carter, B. R., Feely, R. A., van Heuven, S., Hoppema, M., et al. (2019a). The oceanic sink for anthropogenic CO 2 from 1994 to 2007. *Science (80-.).* 363, 1193–1199. doi:10.1126/science.aau5153.
Gruber, N., Clement, D., Carter, B. R. R., Feely, R. A. A., van Heuven, S., Hoppema, M., et al. (2019b). The oceanic sink for anthropogenic CO2 from 1994 to 2007. *Science (80-.).* 363, 1193–1199. doi:10.1126/science.aau5153.
Gruber, N., Gloor, M., Mikaloff Fletcher, S. E., Doney, S. C., Dutkiewicz, S., Follows, M. J., et al. (2009). Oceanic sources, sinks, and transport of atmospheric CO2. *Global Biogeochem. Cycles* 23. doi:https://doi.org/10.1029/2008GB003349.
Gruber, N., and Keeling, C. D. (2001). An improved estimate of the isotopic air-sea disequilibrium of CO2: Implications for the oceanic uptake of anthropogenic CO2. *Geophys. Res. Lett.* 28, 555–558.

doi:https://doi.org/10.1029/2000GL011853.
Gruber, N., Landschützer, P., and Lovenduski, N. S. (2019c). The variable Southern Ocean carbon sink. *Ann. Rev. Mar. Sci.* 11, 159–186. doi:10.1146/annurev-marine-121916-063407.
Gu, J., Yuan, M., Liu, J., Hao, Y., Zhou, Y., Qu, D., et al. (2017). Trade-off between soil organic carbon sequestration and nitrous oxide emissions from winter wheat-summer maize rotations: Implications of a 25-year fertilization experiment in Northwestern China. *Sci. Total Environ.* 595, 371–379. doi:10.1016/j.scitotenv.2017.03.280.
Hansis, E., Davis, S. J., and Pongratz, J. (2015). Relevance of methodological choices for accounting of land use change carbon fluxes. *Global Biogeochem. Cycles*. doi:10.1002/2014GB004997.
Harper, A. B., Powell, T., Cox, P. M., House, J., Huntingford, C., Lenton, T. M., et al. (2018). Land-use emissions play a critical role in land-based mitigation for Paris climate targets. *Nat. Commun.* 9, 2938. doi:10.1038/s41467-018-05340-z.
Harris, I., Jones, P. D., Osborn, T. J., and Lister, D. H. (2014). Updated high-resolution grids of monthly climatic observations – the CRU TS3.10 Dataset. *Int. J. Climatol.* 34, 623–642. doi:10.1002/joc.3711.
Hartmann, J., West, A. J., Renforth, P., Köhler, P., De La Rocha, C. L., Wolf-Gladrow, D. A., et al. (2013). Enhanced chemical weathering as a geoengineering strategy to reduce atmospheric carbon dioxide, supply nutrients, and mitigate ocean acidification. *Rev. Geophys.* 51, 113–149. doi:10.1002/rog.20004.
Hauck, J., Köhler, P., Wolf-Gladrow, D., and Völker, C. (2016). Iron fertilisation and century-scale effects of open ocean dissolution of olivine in a simulated CO2 removal experiment. *Environ. Res. Lett.* 11, 024007. doi:10.1088/1748-9326/11/2/024007.
Hauck, J., Zeising, M., Le Quéré, C., Gruber, N., Bakker, D. C. E., Bopp, L., et al. (2020). Consistency and Challenges in the Ocean Carbon Sink Estimate for the Global Carbon Budget. *Front. Mar. Sci.* 7, 852. doi:10.3389/fmars.2020.571720.
Hauri, C., Doney, S. C., Takahashi, T., Erickson, M., Jiang, G., and Ducklow, H. W. (2015). Two decades of inorganic carbon dynamics along the West Antarctic Peninsula. *Biogeosciences* 12, 6761–6779. doi:10.5194/bg-12-6761-2015.
Heck, V., Gerten, D., Lucht, W., and Boysen, L. R. (2016). Is extensive terrestrial carbon dioxide removal a 'green' form of geoengineering? A global modelling study. *Glob. Planet. Change* 137, 123–130. doi:10.1016/j.gloplacha.2015.12.008.
Heck, V., Gerten, D., Lucht, W., and Popp, A. (2018). Biomass-based negative emissions difficult to reconcile with planetary boundaries. *Nat. Clim. Chang.* 8, 151–155. doi:10.1038/s41558-017-0064-y.
Helbig, M., Waddington, J. M., Alekseychik, P., Amiro, B., Aurela, M., Barr, A. G., et al. (2020). The biophysical climate mitigation potential of boreal peatlands during the growing season. *Environ. Res. Lett.* 15. doi:10.1088/1748-9326/abab34.
Hemes, K. S., Chamberlain, S. D., Eichelmann, E., Anthony, T., Valach, A., Kasak, K., et al. (2019). Assessing the carbon and climate benefit of restoring degraded agricultural peat soils to managed wetlands. *Agric. For. Meteorol.* 268, 202–214. doi:10.1016/j.agrformet.2019.01.017.
Hemes, K. S., Eichelmann, E., Chamberlain, S. D., Knox, S. H., Oikawa, P. Y., Sturtevant, C., et al. (2018). A Unique Combination of Aerodynamic and Surface Properties Contribute to Surface Cooling in Restored Wetlands of the Sacramento-San Joaquin Delta, California. *J. Geophys. Res. Biogeosciences* 123, 2072–2090. doi:https://doi.org/10.1029/2018JG004494.
Hersbach, H., Bell, B., Berrisford, P., Hirahara, S., Horányi, A., Muñoz-Sabater, J., et al. (2020). The ERA5 global reanalysis. *Q. J. R. Meteorol. Soc.* 146, 1999–2049. doi:10.1002/qj.3803.
Holl, D., Pfeiffer, E.-M., and Kutzbach, L. (2020). Comparison of eddy covariance CO2 and CH4 fluxes from mined and recently rewetted sections in a northwestern German cutover bog. *Biogeosciences* 17, 2853–2874. doi:10.5194/bg-17-2853-2020.
Houghton, R. A., and Nassikas, A. A. (2017). Global and regional fluxes of carbon from land use and land cover change 1850-2015. *Global Biogeochem. Cycles* 31, 456–472. doi:10.1002/2016GB005546.
Huang, Y., Wang, C., Lin, C., Zhang, Y., Chen, X., Tang, L., et al. (2019). Methane and Nitrous Oxide Flux after Biochar Application in Subtropical Acidic Paddy Soils under Tobacco-Rice Rotation. *Sci. Rep.* 9, 17277. doi:10.1038/s41598-019-53044-1.
Hugelius, G., Bockheim, J. G., Camill, P., Elberling, B., Grosse, G., Harden, J. W., et al. (2013). A new data set for estimating organic carbon storage to 3 m depth in soils of the northern circumpolar permafrost region. *Earth Syst. Sci. Data* 5, 393–402. doi:10.5194/essd-5-393-2013.
Iida, Y., Takatani, Y., Kojima, A., and Ishii, M. (2020). Global trends of ocean CO2 sink and ocean acidification: an observation-based reconstruction of surface ocean inorganic carbon variables. *J. Oceanogr.* doi:10.1007/s10872-020-00571-5.
IPCC (2019). IPCC Special Report on the Ocean and Cryosphere in a Changing Climate. , eds. H.-O. Pörtner, D. C.

Roberts, V. Masson-Delmotte, P. Zhai, M. Tignor, E. Poloczanska, et al. In Press Available at: https://www.ipcc.ch/report/srocc.

Ishii, M., Kosugi, N., Sasano, D., Saito, S., Midorikawa, T., and Inoue, H. Y. (2011). Ocean acidification off the south coast of Japan: A result from time series observations of CO2 parameters from 1994 to 2008. *J. Geophys. Res.* 116, C06022. doi:10.1029/2010JC006831.

Ishii, M., Rodgers, K. B., Inoue, H. Y., Toyama, K., Sasano, D., Kosugi, N., et al. (2020). Ocean Acidification From Below in the Tropical Pacific. *Global Biogeochem. Cycles* 34, e2019GB006368. doi:10.1029/2019GB006368.

Ishijima, K., Sugawara, S., Kawamura, K., Hashida, G., Morimoto, S., Murayama, S., et al. (2007). Temporal variations of the atmospheric nitrous oxide concentration and its δ15N and δ18O for the latter half of the 20th century reconstructed from firn air analyses. *J. Geophys. Res.* 112, D03305. doi:10.1029/2006JD007208.

Ishizawa, M., Mabuchi, K., Shirai, T., Inoue, M., Morino, I., Uchino, O., et al. (2016). Inter-annual variability of summertime CO 2 exchange in Northern Eurasia inferred from GOSAT XCO 2. *Environ. Res. Lett.* 11, 105001. doi:10.1088/1748-9326/11/10/105001.

Jacobson, A. R., Mikaloff Fletcher, S. E., Gruber, N., Sarmiento, J. L., and Gloor, M. (2007). A joint atmosphere-ocean inversion for surface fluxes of carbon dioxide: 1. Methods and global-scale fluxes. *Global Biogeochem. Cycles* 21. doi:10.1029/2005GB002556.

Jeffery, S., Verheijen, F. G. A., Kammann, C., and Abalos, D. (2016). Biochar effects on methane emissions from soils: A meta-analysis. *Soil Biol. Biochem.* 101, 251–258. doi:10.1016/j.soilbio.2016.07.021.

Jia, G., Shevliakova, E., Artaxo, P., Noblet-Ducoudré, N. De, Houghton, R., House, J., et al. (2019). "Land–climate interactions," in *Climate Change and Land: an IPCC special report on climate change, desertification, land degradation, sustainable land management, food security, and greenhouse gas fluxes in terrestrial ecosystems.*, eds. P. R. Shukla, J. Skea, E. C. Buendia, V. Masson-Delmotte, H.-O. Pörtner, D. C. Roberts, et al. (In Press), 131–248. Available at: https://www.ipcc.ch/srccl/chapter/chapter-2.

Jiang, L.-Q., Carter, B. R., Feely, R. A., Lauvset, S. K., and Olsen, A. (2019). Surface ocean pH and buffer capacity: past, present and future. *Sci. Rep.* 9, 18624. doi:10.1038/s41598-019-55039-4.

Jin, X., and Gruber, N. (2003). Offsetting the radiative benefit of ocean iron fertilization by enhancing N 2 O emissions. *Geophys. Res. Lett.* 30, 2249. doi:10.1029/2003GL018458.

Jones, C. D., Ciais, P., Davis, S. J., Friedlingstein, P., Gasser, T., Peters, G. P., et al. (2016). Simulating the earth system response to negative emissions. *Environ. Res. Lett.* 11, 095012. doi:10.1088/1748-9326/11/9/095012.

Joos, F., Meyer, R., Bruno, M., and Leuenberger, M. (1999). The variability in the carbon sinks as reconstructed for the last 1000 years. *Geophys. Res. Lett.* 26, 1437–1440. doi:https://doi.org/10.1029/1999GL900250.

Kammann, C., Ippoloto, J., Hagemann, N., Borchard, N., Cayuela, M. L., Estavillo, J. M., et al. (2017). Biochar as a Tool to teduce the Agricultural Greenhouse-gas Burden – Knowns, Unknowns and Future Research Needs. *J. Environ. Eng. Landsc. Manag.* 25, 114–139. doi:10.3846/16486897.2017.1319375.

Kantola, I. B., Masters, M. D., Beerling, D. J., Long, S. P., and DeLucia, E. H. (2017). Potential of global croplands and bioenergy crops for climate change mitigation through deployment for enhanced weathering. *Biol. Lett.* 13, 20160714. doi:10.1098/rsbl.2016.0714.

Karhu, K., Mattila, T., Bergström, I., and Regina, K. (2011). Biochar addition to agricultural soil increased CH4 uptake and water holding capacity – Results from a short-term pilot field study. *Agric. Ecosyst. Environ.* 140, 309–313. doi:https://doi.org/10.1016/j.agee.2010.12.005.

Kaushal, S. S., Likens, G. E., Pace, M. L., Utz, R. M., Haq, S., Gorman, J., et al. (2018). Freshwater salinization syndrome on a continental scale. *Proc. Natl. Acad. Sci.* 115, E574–E583. doi:10.1073/pnas.1711234115.

Keeling, C. D., Whorf, T. P., Wahlen, M., and van der Plicht, J. (2001). Exchanges of Atmospheric CO2 and 13CO2 with the Terrestrial Biosphere and Oceans from 1978 to 2000. I. Global Aspects. San Diego, CA, USA: Scripps Institution of Oceanography, University of California San Diego Available at: https://escholarship.org/uc/item/09v319r9.

Keeling, R. F., and Manning, A. C. (2014). "Studies of Recent Changes in Atmospheric O2 Content," in *Treatise on Geochemistry (Second Edition)*, eds. H. D. Holland and K. K. Turekian (Elsevier), 385–404. doi:10.1016/B978-0-08-095975-7.00420-4.

Keller, D. P., Feng, E. Y., and Oschlies, A. (2014a). Potential climate engineering effectiveness and side effects during a high carbon dioxide-emission scenario. *Nat. Commun.* 5, 3304. doi:10.1038/ncomms4304.

Keller, D. P., Feng, E. Y., and Oschlies, A. (2014b). Potential climate engineering effectiveness and side effects during a high carbon dioxide-emission scenario. *Nat. Commun.* 5, 3304. doi:10.1038/ncomms4304.

Keller, D. P., Lenton, A., Littleton, E. W., Oschlies, A., Scott, V., and Vaughan, N. E. (2018). The Effects of Carbon Dioxide Removal on the Carbon Cycle. *Curr. Clim. Chang. Reports* 4, 250–265. doi:10.1007/s40641-018-0104-3.

Key, R. M., Kozyr, A., Sabine, C. L., Lee, K., Wanninkhof, R., Bullister, J. L., et al. (2004). A global ocean carbon climatology: Results from Global Data Analysis Project (GLODAP). *Global Biogeochem. Cycles* 18, GB4031.

doi:10.1029/2004GB002247.
Kirschke, S., Bousquet, P., Ciais, P., Saunois, M., Canadell, J. G., Dlugokencky, E. J., et al. (2013). Three decades of global methane sources and sinks. *Nat. Geosci.* 6, 813–823. doi:10.1038/ngeo1955.
Kitidis, V., Brown, I., Hardman-Mountford, N., and Lefèvre, N. (2017). Surface ocean carbon dioxide during the Atlantic Meridional Transect (1995–2013); evidence of ocean acidification. *Prog. Oceanogr.* 158, 65–75. doi:https://doi.org/10.1016/j.pocean.2016.08.005.
Kluber, L. A., Miller, J. O., Ducey, T. F., Hunt, P. G., Lang, M., and S. Ro, K. (2014). Multistate assessment of wetland restoration on CO2 and N2O emissions and soil bacterial communities. *Appl. Soil Ecol.* 76, 87–94. doi:10.1016/j.apsoil.2013.12.014.
Kobayashi, S., OTA, Y., HARADA, Y., EBITA, A., MORIYA, M., ONODA, H., et al. (2015). The JRA-55 Reanalysis: General Specifications and Basic Characteristics. *J. Meteorol. Soc. Japan. Ser. II* 93, 5–48. doi:10.2151/jmsj.2015-001.
Köhler, P., Abrams, J. F., Völker, C., Hauck, J., and Wolf-Gladrow, D. A. (2013). Geoengineering impact of open ocean dissolution of olivine on atmospheric CO2, surface ocean pH and marine biology. *Environ. Res. Lett.* 8, 014009. doi:10.1088/1748-9326/8/1/014009.
Koskinen, M., Tahvanainen, T., Sarkkola, S., Menberu, M. W., Laurén, A., Sallantaus, T., et al. (2017). Restoration of nutrient-rich forestry-drained peatlands poses a risk for high exports of dissolved organic carbon, nitrogen, and phosphorus. *Sci. Total Environ.* 586, 858–869. doi:10.1016/j.scitotenv.2017.02.065.
Krakauer, N. Y., Randerson, J. T., Primeau, F. W., Gruber, N., and Menemenlis, D. (2006). Carbon isotope evidence for the latitudinal distribution and wind speed dependence of the air–sea gas transfer velocity. *Tellus B Chem. Phys. Meteorol.* 58, 390–417. doi:10.1111/j.1600-0889.2006.00223.x.
Krause, A., Pugh, T. A. M., Bayer, A. D., Doelman, J. C., Humpenöder, F., Anthoni, P., et al. (2017). Global consequences of afforestation and bioenergy cultivation on ecosystem service indicators. *Biogeosciences* 14, 4829–4850. doi:10.5194/bg-14-4829-2017.
Kraxner, F., Nordström, E.-M., Havlík, P., Gusti, M., Mosnier, A., Frank, S., et al. (2013). Global bioenergy scenarios – Future forest development, land-use implications, and trade-offs. *Biomass and Bioenergy* 57, 86–96. doi:10.1016/j.biombioe.2013.02.003.
Kwiatkowski, L., Ricke, K. L., and Caldeira, K. (2015). Atmospheric consequences of disruption of the ocean thermocline. *Environ. Res. Lett.* 10, 034016. doi:10.1088/1748-9326/10/3/034016.
Lampitt, R. ., Achterberg, E. ., Anderson, T. ., Hughes, J. ., Iglesias-Rodriguez, M. ., Kelly-Gerreyn, B. ., et al. (2008). Ocean fertilization: a potential means of geoengineering? *Philos. Trans. R. Soc. A Math. Phys. Eng. Sci.* 366, 3919–3945. doi:10.1098/rsta.2008.0139.
Landschützer, P., Gruber, N., and Bakker, D. C. E. (2016). Decadal variations and trends of the global ocean carbon sink. *Global Biogeochem. Cycles* 30, 1396–1417. doi:10.1002/2015GB005359.
Landschützer, P., Gruber, N., and Bakker, D. C. E. (2020a). An observation-based global monthly gridded sea surface pCO2 product from 1982 onward and its monthly climatology (NCEI Accession 0160558). *NOAA Natl. Centers Environ. Inf.*, Version 5.5. doi:10.7289/v5z899n6.
Landschützer, P., Gruber, N., Bakker, D. C. E., and Schuster, U. (2014). Recent variability of the global ocean carbon sink. *Global Biogeochem. Cycles* 28, 927–949. doi:10.1002/2014GB004853.
Landschützer, P., Gruber, N., Bakker, D. C. E., Stemmler, I., and Six, K. D. (2018). Strengthening seasonal marine CO2 variations due to increasing atmospheric CO2. *Nat. Clim. Chang.* 8, 146–150. doi:10.1038/s41558-017-0057-x.
Landschützer, P., Laruelle, G. G., Roobaert, A., and Regnier, P. (2020b). A uniform pCO2 climatology combining open and coastal oceans. *Earth Syst. Sci. Data* 12, 2537–2553. doi:10.5194/essd-12-2537-2020.
Laruelle, G. G., Landschützer, P., Gruber, N., Tison, J.-L., Delille, B., and Regnier, P. (2017). Global high-resolution monthly CO2 climatology for the coastal ocean derived from neural network interpolation. *Biogeosciences* 14, 4545–4561. doi:10.5194/bg-14-4545-2017.
Lauvset, S. K., Carter, B. R., Perez, F. F., Jiang, L. -Q., Feely, R. A., Velo, A., et al. (2020). Processes driving global interior ocean pH distribution. *Global Biogeochem. Cycles*, 2019GB006229. doi:10.1029/2019GB006229.
Lauvset, S. K., and Gruber, N. (2014). Long-term trends in surface ocean pH in the North Atlantic. *Mar. Chem.* 162, 71–76. doi:https://doi.org/10.1016/j.marchem.2014.03.009.
Lauvset, S. K., Gruber, N., Landschützer, P., Olsen, A., and Tjiputra, J. (2015). Trends and drivers in global surface ocean pH over the past 3 decades. *Biogeosciences* 12, 1285–1298. doi:10.5194/bg-12-1285-2015.
Lauvset, S. K., Key, R. M., Olsen, A., van Heuven, S., Velo, A., Lin, X., et al. (2016). A new global interior ocean mapped climatology: the 1° × 1° GLODAP version 2. *Earth Syst. Sci. Data* 8, 325–340. doi:10.5194/essd-8-325-2016.
Law, R. M., Ziehn, T., Matear, R. J., Lenton, A., Chamberlain, M. A., Stevens, L. E., et al. (2017). The carbon cycle in the Australian Community Climate and Earth System Simulator (ACCESS-ESM1) – Part 1: Model description and pre-

industrial simulation. *Geosci. Model Dev.* 10, 2567–2590. doi:10.5194/gmd-10-2567-2017.
Liao, E., Resplandy, L., Liu, J., and Bowman, K. W. (2020). Amplification of the Ocean Carbon Sink During El Niños: Role of Poleward Ekman Transport and Influence on Atmospheric CO2. *Global Biogeochem. Cycles* 34, e2020GB006574. doi:https://doi.org/10.1029/2020GB006574.
Liu, C., Wang, H., Tang, X., Guan, Z., Reid, B. J., Rajapaksha, A. U., et al. (2016). Biochar increased water holding capacity but accelerated organic carbon leaching from a sloping farmland soil in China. *Environ. Sci. Pollut. Res.* 23, 995–1006. doi:10.1007/s11356-015-4885-9.
Liu, H., Wrage-Mönnig, N., and Lennartz, B. (2020). Rewetting strategies to reduce nitrous oxide emissions from European peatlands. *Commun. Earth Environ.* 1, 17. doi:10.1038/s43247-020-00017-2.
Liu, Z., He, T., Cao, T., Yang, T., Meng, J., and Chen, W. (2017). Effects of biochar application on nitrogen leaching, ammonia volatilization and nitrogen use efficiency in two distinct soils. *J. soil Sci. plant Nutr.* 17, 515–528. doi:10.4067/S0718-95162017005000037.
Loulergue, L., Schilt, A., Spahni, R., Masson-Delmotte, V., Blunier, T., Lemieux, B., et al. (2008). Orbital and millennial-scale features of atmospheric CH4 over the past 800,000 years. *Nature* 453, 383–386. doi:10.1038/nature06950.
Lundin, L., Nilsson, T., Jordan, S., Lode, E., and Strömgren, M. (2017). Impacts of rewetting on peat, hydrology and water chemical composition over 15 years in two finished peat extraction areas in Sweden. *Wetl. Ecol. Manag.* 25, 405–419. doi:10.1007/s11273-016-9524-9.
Marcellin Yao, K., Marcou, O., Goyet, C., Guglielmi, V., Touratier, F., and Savy, J.-P. (2016). Time variability of the north-western Mediterranean Sea pH over 1995–2011. *Mar. Environ. Res.* 116, 51–60. doi:https://doi.org/10.1016/j.marenvres.2016.02.016.
McGillis, W. R., Edson, J. B., Hare, J. E., and Fairall, C. W. (2001). Direct covariance air-sea CO 2 fluxes. *J. Geophys. Res. Ocean.* 106, 16729–16745. doi:10.1029/2000JC000506.
McKinley, G. A., Fay, A. R., Eddebbar, Y. A., Gloege, L., and Lovenduski, N. S. (2020). External Forcing Explains Recent Decadal Variability of the Ocean Carbon Sink. *AGU Adv.* 1. doi:10.1029/2019AV000149.
McKinley, G. A., Fay, A. R., Lovenduski, N. S., and Pilcher, D. J. (2017). Natural Variability and Anthropogenic Trends in the Ocean Carbon Sink. *Ann. Rev. Mar. Sci.* 9, 125–150. doi:10.1146/annurev-marine-010816-060529.
McNeil, B. I., Matear, R. J., Key, R. M., Bullister, J. L., and Sarmiento, J. L. (2003). Anthropogenic CO₂ Uptake by the Ocean Based on the Global Chlorofluorocarbon Data Set. *Science (80-.).* 299, 235. doi:10.1126/science.1077429.
McNorton, J., Wilson, C., Gloor, M., Parker, R. J., Boesch, H., Feng, W., et al. (2018). Attribution of recent increases in atmospheric methane through 3-D inverse modelling. *Atmos. Chem. Phys.* 18, 18149–18168. doi:10.5194/acp-18-18149-2018.
Meinshausen, M., Vogel, E., Nauels, A., Lorbacher, K., Meinshausen, N., Etheridge, D. M., et al. (2017). Historical greenhouse gas concentrations for climate modelling (CMIP6). *Geosci. Model Dev.* 10, 2057–2116. doi:10.5194/gmd-10-2057-2017.
Meli, P., Rey Benayas, J. M., Balvanera, P., and Martínez Ramos, M. (2014). Restoration enhances wetland biodiversity and ecosystem service supply, but results are context-dependent: a meta-analysis. *PLoS One* 9, e93507–e93507. doi:10.1371/journal.pone.0093507.
Mengis, N., Keller, D. P., Rickels, W., Quaas, M., and Oschlies, A. (2019). Climate engineering–induced changes in correlations between Earth system variables—implications for appropriate indicator selection. *Clim. Change* 153, 305–322. doi:10.1007/s10584-019-02389-7.
Merlivat, L., Boutin, J., Antoine, D., Beaumont, L., Golbol, M., and Vellucci, V. (2018). Increase of dissolved inorganic carbon and decrease in pH in near-surface waters in the Mediterranean Sea during the past two decades. *Biogeosciences* 15, 5653–5662. doi:10.5194/bg-15-5653-2018.
Midorikawa, T., Ishii, M., Kosugi, N., Sasano, D., Nakano, T., Saito, S., et al. (2012). Recent deceleration of oceanic pCO2 increase in the western North Pacific in winter. *Geophys. Res. Lett.* 39, n/a-n/a. doi:10.1029/2012GL051665.
Mikaloff Fletcher, S. E., Gruber, N., Jacobson, A. R., Doney, S. C., Dutkiewicz, S., Gerber, M., et al. (2006). Inverse estimates of anthropogenic CO2 uptake, transport, and storage by the ocean. *Global Biogeochem. Cycles* 20. doi:https://doi.org/10.1029/2005GB002530.
Molari, M., Guilini, K., Lott, C., Weber, M., de Beer, D., Meyer, S., et al. (2018). CO2 leakage alters biogeochemical and ecological functions of submarine sands. *Sci. Adv.* 4, eaao2040. doi:10.1126/sciadv.aao2040.
Müller, S. A., Joos, F., Plattner, G.-K., Edwards, N. R., and Stocker, T. F. (2008). Modeled natural and excess radiocarbon: Sensitivities to the gas exchange formulation and ocean transport strength. *Global Biogeochem. Cycles* 22, n/a-n/a. doi:10.1029/2007GB003065.
Naegler, T. (2009). Reconciliation of excess 14 C-constrained global CO 2 piston velocity estimates. *Tellus B Chem. Phys. Meteorol.* 61, 372–384. doi:10.1111/j.1600-0889.2008.00408.x.

Nakano, H., Ishii, M., Rodgers, K. B., Tsujino, H., and Yamanaka, G. (2015). Anthropogenic CO2 uptake, transport, storage, and dynamical controls in the ocean imposed by the meridional overturning circulation: A modeling study. *Global Biogeochem. Cycles* 29, 1706–1724. doi:10.1002/2015GB005128.

Nakazawa, T., Morimoto, S., Aoki, S., and Tanaka, M. (1997). Temporal and spatial variations of the carbon isotopic ratio of atmospheric carbon dioxide in the western Pacific region. *J. Geophys. Res. Atmos.* 102, 1271–1285. doi:10.1029/96JD02720.

NASEM (2019). Negative Emissions Technologies and Reliable Sequestration: A Research Agenda. Washington, DC, USA: National Academies of Sciences, Engineering, and Medicine (NASEM). The National Academies Press doi:10.17226/25259.

Nightingale, P. D., Malin, G., Law, C. S., Watson, A. J., Liss, P. S., Liddicoat, M. I., et al. (2000). In situ evaluation of air-sea gas exchange parameterizations using novel conservative and volatile tracers. *Global Biogeochem. Cycles* 14, 373–387. doi:10.1029/1999GB900091.

Nisbet, E. G., Fisher, R. E., Lowry, D., France, J. L., Allen, G., Bakkaloglu, S., et al. (2020). Methane Mitigation: Methods to Reduce Emissions, on the Path to the Paris Agreement. *Rev. Geophys.* 58, e2019RG000675. doi:https://doi.org/10.1029/2019RG000675.

Niwa, Y., Tomita, H., Satoh, M., Imasu, R., Sawa, Y., Tsuboi, K., et al. (2017). A 4D-Var inversion system based on the icosahedral grid model (NICAM-TM 4D-Var v1.0) – Part 1: Offline forward and adjoint transport models. *Geosci. Model Dev.* 10, 1157–1174. doi:10.5194/gmd-10-1157-2017.

Olafsson, J., Olafsdottir, S. R., Benoit-Cattin, A., Danielsen, M., Arnarson, T. S., and Takahashi, T. (2009). Rate of Iceland Sea acidification from time series measurements. *Biogeosciences* 6, 2661–2668. doi:10.5194/bg-6-2661-2009.

Olefeldt, D., Goswami, S., Grosse, G., Hayes, D. J., Hugelius, G., Kuhry, P., et al. (2016). Arctic Circumpolar Distribution and Soil Carbon of Thermokarst Landscapes, 2015. doi:10.3334/ORNLDAAC/1332.

Olsen, A., Key, R. M., van Heuven, S., Lauvset, S. K., Velo, A., Lin, X., et al. (2016). The Global Ocean Data Analysis Project version 2 (GLODAPv2) – an internally consistent data product for the world ocean. *Earth Syst. Sci. Data* 8, 297–323. doi:10.5194/essd-8-297-2016.

Ono, H., Kosugi, N., Toyama, K., Tsujino, H., Kojima, A., Enyo, K., et al. (2019). Acceleration of ocean acidification in the Western North Pacific. *Geophys. Res. Lett.* 46, 13161–13169. doi:10.1029/2019GL085121.

Oschlies, A. (2009). Impact of atmospheric and terrestrial CO2 feedbacks on fertilization-induced marine carbon uptake. *Biogeosciences* 6, 1603–1613. doi:10.5194/bg-6-1603-2009.

Oschlies, A., Koeve, W., Rickels, W., and Rehdanz, K. (2010a). Side effects and accounting aspects of hypothetical large-scale Southern Ocean iron fertilization. *Biogeosciences* 7, 4017–4035. doi:10.5194/bg-7-4017-2010.

Oschlies, A., Pahlow, M., Yool, A., and Matear, R. J. (2010b). Climate engineering by artificial ocean upwelling: Channelling the sorcerer's apprentice. *Geophys. Res. Lett.* 37. doi:10.1029/2009GL041961.

Oschlies, A., Pahlow, M., Yool, A., and Matear, R. J. (2010c). Climate engineering by artificial ocean upwelling: Channelling the sorcerer's apprentice. *Geophys. Res. Lett.* 37, L04701. doi:10.1029/2009GL041961.

Park, S., Croteau, P., Boering, K. A., Etheridge, D. M., Ferretti, D., Fraser, P. J., et al. (2012). Trends and seasonal cycles in the isotopic composition of nitrous oxide since 1940. *Nat. Geosci.* 5, 261–265. doi:10.1038/ngeo1421.

Patra, P. K., Takigawa, M., Watanabe, S., Chandra, N., Ishijima, K., and Yamashita, Y. (2018). Improved Chemical Tracer Simulation by MIROC4.0-based Atmospheric Chemistry-Transport Model (MIROC4-ACTM). *SOLA* 14, 91–96. doi:10.2151/sola.2018-016.

Paulsen, H., Ilyina, T., Six, K. D., and Stemmler, I. (2017). Incorporating a prognostic representation of marine nitrogen fixers into the global ocean biogeochemical model HAMOCC. *J. Adv. Model. Earth Syst.* 9, 438–464. doi:10.1002/2016MS000737.

Paustian, K., Larson, E., Kent, J., Marx, E., and Swan, A. (2019). Soil C Sequestration as a Biological Negative Emission Strategy. *Front. Clim.* 1, 8. doi:10.3389/fclim.2019.00008.

Paustian, K., Lehmann, J., Ogle, S., Reay, D., Robertson, G. P., and Smith, P. (2016). Climate-smart soils. *Nature* 532, 49–57. doi:10.1038/nature17174.

Pongratz, J., Reick, C. H., Raddatz, T., and Claussen, M. (2010). Biogeophysical versus biogeochemical climate response to historical anthropogenic land cover change. *Geophys. Res. Lett.* 37, L08702. doi:10.1029/2010GL043010.

Prentice, I. C., Farquhar, G. D., Fasham, M. J. R., Goulden, M. L., Heimann, M., Jaramillo, V. J., et al. (2001). "The carbon cycle and atmospheric carbon dioxide.," in *Climate change 2001: The scientific basis. Contribution of Working Group I to the Third Assessment Report of the Intergovernmental Panel on Climate Change (IPCC).*, eds. J. T. Houghton, Y. Ding, D. J. Griggs, M. Noguer, P. J. van der Linden, X. Dai, et al. (Cambridge University Press, Cambridge, United Kingdom and New York, NY, USA), 183–237.

Prinn, R. G., Weiss, R. F., Arduini, J., Arnold, T., DeWitt, H. L., Fraser, P. J., et al. (2018). History of chemically and radiatively important atmospheric gases from the Advanced Global Atmospheric Gases Experiment (AGAGE). *Earth*

Syst. Sci. Data 10, 985–1018. doi:10.5194/essd-10-985-2018.
Prokopiou, M., Martinerie, P., Sapart, C. J., Witrant, E., Monteil, G., Ishijima, K., et al. (2017). Constraining N2O emissions since 1940 using firn air isotope measurements in both hemispheres. *Atmos. Chem. Phys.* 17, 4539–4564. doi:10.5194/acp-17-4539-2017.
Ramon, J., Lledó, L., Torralba, V., Soret, A., and Doblas-Reyes, F. J. (2019). What global reanalysis best represents near-surface winds? *Q. J. R. Meteorol. Soc.* 145, 3236–3251. doi:10.1002/qj.3616.
Rayner, N. A. (2003). Global analyses of sea surface temperature, sea ice, and night marine air temperature since the late nineteenth century. *J. Geophys. Res.* 108, 4407. doi:10.1029/2002JD002670.
Renforth, P., and Henderson, G. (2017). Assessing ocean alkalinity for carbon sequestration. *Rev. Geophys.* 55, 636–674. doi:10.1002/2016RG000533.
Renou-Wilson, F., Moser, G., Fallon, D., Farrell, C. A., Müller, C., and Wilson, D. (2019). Rewetting degraded peatlands for climate and biodiversity benefits: Results from two raised bogs. *Ecol. Eng.* 127, 547–560. doi:10.1016/j.ecoleng.2018.02.014.
Resplandy, L., Keeling, R. F., Rödenbeck, C., Stephens, B. B., Khatiwala, S., Rodgers, K. B., et al. (2018). Revision of global carbon fluxes based on a reassessment of oceanic and riverine carbon transport. *Nat. Geosci.* 11, 504–509. doi:10.1038/s41561-018-0151-3.
Rice, A. L., Butenhoff, C. L., Teama, D. G., Röger, F. H., Khalil, M. A. K., and Rasmussen, R. A. (2016). Atmospheric methane isotopic record favors fossil sources flat in 1980s and 1990s with recent increase. *Proc. Natl. Acad. Sci.* 113, 10791–10796. doi:10.1073/pnas.1522923113.
Rödenbeck, C., Bakker, D. C. E., Gruber, N., Iida, Y., Jacobson, A. R., Jones, S., et al. (2015). Data-based estimates of the ocean carbon sink variability – first results of the Surface Ocean pCO2 Mapping intercomparison (SOCOM). *Biogeosciences* 12, 7251–7278. doi:10.5194/bg-12-7251-2015.
Rödenbeck, C., Bakker, D. C. E., Metzl, N., Olsen, A., Sabine, C., Cassar, N., et al. (2014). Interannual sea–air CO2 flux variability from an observation-driven ocean mixed-layer scheme. *Biogeosciences* 11, 4599–4613. doi:10.5194/bg-11-4599-2014.
Rödenbeck, C., Keeling, R. F., Bakker, D. C. E., Metzl, N., Olsen, A., Sabine, C., et al. (2013). Global surface-ocean pCO2 and sea–air CO2 flux variability from an observation-driven ocean mixed-layer. *Ocean Sci.* 9, 193–216. doi:10.5194/os-9-193-2013.
Rödenbeck, C., Zaehle, S., Keeling, R., and Heimann, M. (2018). How does the terrestrial carbon exchange respond to inter-annual climatic variations? A quantification based on atmospheric CO₂ data. *Biogeosciences* 15, 2481–2498. doi:10.5194/bg-15-2481-2018.
Roe, S., Streck, C., Obersteiner, M., Frank, S., Griscom, B., Drouet, L., et al. (2019a). Contribution of the land sector to a 1.5 °C world. *Nat. Clim. Chang.* 9, 817–828. doi:10.1038/s41558-019-0591-9.
Roe, S., Streck, C., Obersteiner, M., Frank, S., Griscom, B., Drouet, L., et al. (2019b). Contribution of the land sector to a 1.5 °C world. *Nat. Clim. Chang.* 9, 817–828. doi:10.1038/s41558-019-0591-9.
Roobaert, A., Laruelle, G. G., Landschützer, P., and Regnier, P. (2018). Uncertainty in the global oceanic CO2 uptake induced by wind forcing: quantification and spatial analysis. *Biogeosciences* 15, 1701–1720. doi:10.5194/bg-15-1701-2018.
Rosentreter, J. A., Maher, D. T., Erler, D. V., Murray, R. H., and Eyre, B. D. (2018). Methane emissions partially offset "blue carbon" burial in mangroves. *Sci. Adv.* 4, eaao4985. doi:10.1126/sciadv.aao4985.
Rubino, M., Etheridge, D. M., Thornton, D. P., Howden, R., Allison, C. E., Francey, R. J., et al. (2019). Revised records of atmospheric trace gases CO2, CH4, N2O, and 13C over the last 2000 years from Law Dome, Antarctica. *Earth Syst. Sci. Data* 11, 473–492. doi:10.5194/essd-11-473-2019.
Saeki, T., and Patra, P. K. (2017). Implications of overestimated anthropogenic CO2 emissions on East Asian and global land CO2 flux inversion. *Geosci. Lett.* 4, 9. doi:10.1186/s40562-017-0074-7.
Sallée, J.-B., Matear, R. J., Rintoul, S. R., and Lenton, A. (2012). Localized subduction of anthropogenic carbon dioxide in the Southern Hemisphere oceans. *Nat. Geosci.* 5, 579–584. doi:10.1038/ngeo1523.
Salter, I., Schiebel, R., Ziveri, P., Movellan, A., Lampitt, R., and Wolff, G. A. (2014). Carbonate counter pump stimulated by natural iron fertilization in the Polar Frontal Zone. *Nat. Geosci.* 7, 885–889. doi:10.1038/ngeo2285.
Saunois, M., Stavert, A. R., Poulter, B., Bousquet, P., Canadell, J. G., Jackson, R. B., et al. (2020). The Global Methane Budget 2000–2017. *Earth Syst. Sci. Data* 12, 1561–1623. doi:10.5194/essd-12-1561-2020.
Schilt, A., Baumgartner, M., Schwander, J., Buiron, D., Capron, E., Chappellaz, J., et al. (2010). Atmospheric nitrous oxide during the last 140,000years. *Earth Planet. Sci. Lett.* 300, 33–43. doi:10.1016/j.epsl.2010.09.027.
Schwinger, J., Goris, N., Tjiputra, J. F., Kriest, I., Bentsen, M., Bethke, I., et al. (2016). Evaluation of NorESM-OC (versions 1 and 1.2), the ocean carbon-cycle stand-alone configuration of the Norwegian Earth System Model

(NorESM1). *Geosci. Model Dev.* 9, 2589–2622. doi:10.5194/gmd-9-2589-2016.
Shen, Q., Hedley, M., Camps Arbestain, M., and Kirschbaum, M. U. . (2016). Can biochar increase the bioavailability of phosphorus? *J. soil Sci. plant Nutr.* 16, 0–0. doi:10.4067/S0718-95162016005000022.
Shutler, J. D., Land, P. E., Piolle, J.-F., Woolf, D. K., Goddijn-Murphy, L., Paul, F., et al. (2016). FluxEngine: A Flexible Processing System for Calculating Atmosphere–Ocean Carbon Dioxide Gas Fluxes and Climatologies. *J. Atmos. Ocean. Technol.* 33, 741–756. doi:10.1175/JTECH-D-14-00204.1.
Singh, N. K., Gourevitch, J. D., Wemple, B. C., Watson, K. B., Rizzo, D. M., Polasky, S., et al. (2019). Optimizing wetland restoration to improve water quality at a regional scale. *Environ. Res. Lett.* 14, 64006. doi:10.1088/1748-9326/ab1827.
Smetacek, V., Klaas, C., Strass, V. H., Assmy, P., Montresor, M., Cisewski, B., et al. (2012). Deep carbon export from a Southern Ocean iron-fertilized diatom bloom. *Nature* 487, 313–319. doi:10.1038/nature11229.
Smith, P. (2016). Soil carbon sequestration and biochar as negative emission technologies. *Glob. Chang. Biol.* 22, 1315–1324. doi:10.1111/gcb.13178.
Smith, P., Adams, J., Beerling, D. J., Beringer, T., Calvin, K. V., Fuss, S., et al. (2019). Land-Management Options for Greenhouse Gas Removal and Their Impacts on Ecosystem Services and the Sustainable Development Goals. *Annu. Rev. Environ. Resour.* 44, 255–286. doi:10.1146/annurev-environ-101718-033129.
Smith, P., Calvin, K., Nkem, J., Campbell, D., Cherubini, F., Grassi, G., et al. (2020). Which practices co-deliver food security, climate change mitigation and adaptation, and combat land degradation and desertification? *Glob. Chang. Biol.* 26, 1532–1575. doi:https://doi.org/10.1111/gcb.14878.
Smith, P., Davis, S. J., Creutzig, F., Fuss, S., Minx, J., Gabrielle, B., et al. (2016). Biophysical and economic limits to negative CO2 emissions. *Nat. Clim. Chang.* 6, 42–50. doi:10.1038/nclimate2870.
Smith, P., Martino, D., Cai, Z., Gwary, D., Janzen, H., Kumar, P., et al. (2008). Greenhouse gas mitigation in agriculture. *Philos. Trans. R. Soc. B Biol. Sci.* 363, 789–813. doi:10.1098/rstb.2007.2184.
Smith, P., Price, J., Molotoks, A., Warren, R., and Malhi, Y. (2018). Impacts on terrestrial biodiversity of moving from a 2°C to a 1.5°C target. *Philos. Trans. R. Soc. A Math. Eng. Sci.* 376, 20160456. doi:10.1098/rsta.2016.0456.
Smith, W. K., Zhao, M., and Running, S. W. (2012). Global bioenergy capacity as constrained by observed biospheric productivity rates. *Bioscience* 62, 911–922. doi:10.1525/bio.2012.62.10.11.
Sonntag, S., Ferrer González, M., Ilyina, T., Kracher, D., Nabel, J. E. M. S., Niemeier, U., et al. (2018). Quantifying and Comparing Effects of Climate Engineering Methods on the Earth System. *Earth's Futur.* 6, 149–168. doi:10.1002/2017EF000620.
Sutton, A. J., Feely, R. A., Sabine, C. L., McPhaden, M. J., Takahashi, T., Chavez, F. P., et al. (2014). Natural variability and anthropogenic change in equatorial Pacific surface ocean pCO2 and pH. *Global Biogeochem. Cycles* 28, 131–145. doi:10.1002/2013GB004679.
Sutton, A. J., Wanninkhof, R., Sabine, C. L., Feely, R. A., Cronin, M. F., and Weller, R. A. (2017). Variability and trends in surface seawater pCO2 and CO2 flux in the Pacific Ocean. *Geophys. Res. Lett.* 44, 5627–5636. doi:10.1002/2017GL073814.
Sweeney, C., Gloor, E., Jacobson, A. R., Key, R. M., McKinley, G., Sarmiento, J. L., et al. (2007). Constraining global air-sea gas exchange for CO 2 with recent bomb 14 C measurements. *Global Biogeochem. Cycles* 21, GB2015. doi:10.1029/2006GB002784.
Takahashi, T., Sutherland, S. C., Chipman, D. W., Goddard, J. G., Ho, C., Newberger, T., et al. (2014). Climatological distributions of pH, pCO2, total CO2, alkalinity, and CaCO3 saturation in the global surface ocean, and temporal changes at selected locations. *Mar. Chem.* 164, 95–125. doi:10.1016/j.marchem.2014.06.004.
Tanhua, T., Hoppema, M., Jones, E. M., Stöven, T., Hauck, J., Dávila, M. G., et al. (2017). Temporal changes in ventilation and the carbonate system in the Atlantic sector of the Southern Ocean. *Deep Sea Res. Part II Top. Stud. Oceanogr.* 138, 26–38. doi:10.1016/j.dsr2.2016.10.004.
Thompson, R. L., Lassaletta, L., Patra, P. K., Wilson, C., Wells, K. C., Gressent, A., et al. (2019). Acceleration of global N2O emissions seen from two decades of atmospheric inversion. *Nat. Clim. Chang.* 9, 993–998. doi:10.1038/s41558-019-0613-7.
Tian, H., Xu, R., Canadell, J. G., Thompson, R. L., Winiwarter, W., Suntharalingam, P., et al. (2020). A comprehensive quantification of global nitrous oxide sources and sinks. *Nature* 586, 248–256. doi:10.1038/s41586-020-2780-0.
Tian, H., Yang, J., Xu, R., Lu, C., Canadell, J. G., Davidson, E. A., et al. (2019). Global soil nitrous oxide emissions since the preindustrial era estimated by an ensemble of terrestrial biosphere models: Magnitude, attribution, and uncertainty. *Glob. Chang. Biol.* 25, 640–659. doi:10.1111/gcb.14514.
Tiemeyer, B., Freibauer, A., Borraz, E. A., Augustin, J., Bechtold, M., Beetz, S., et al. (2020). A new methodology for organic soils in national greenhouse gas inventories: Data synthesis, derivation and application. *Ecol. Indic.* 109, 105838. doi:https://doi.org/10.1016/j.ecolind.2019.105838.
Tohjima, Y., Mukai, H., Machida, T., Hoshina, Y., and Nakaoka, S.-I. (2019). Global carbon budgets estimated from

atmospheric O2/N2 andCO2 observations in the western Pacific region over a 15-year period. *Atmos. Chem. Phys.* 19, 9269–9285. doi:10.5194/acp-19-9269-2019.
Tokarska, K. B., and Zickfeld, K. (2015). The effectiveness of net negative carbon dioxide emissions in reversing anthropogenic climate change. *Environ. Res. Lett.* 10, 094013. doi:10.1088/1748-9326/10/9/094013.
Tonitto, C., David, M. B., and Drinkwater, L. E. (2006). Replacing bare fallows with cover crops in fertilizer-intensive cropping systems: A meta-analysis of crop yield and N dynamics. *Agric. Ecosyst. Environ.* 112, 58–72. doi:10.1016/j.agee.2005.07.003.
Toyama, K., Rodgers, K. B., Blanke, B., Iudicone, D., Ishii, M., Aumont, O., et al. (2017). Large reemergence of anthropogenic carbon into the ocean's surface mixed layer sustained by the ocean's overturning circulation. *J. Clim.* 30, 8615–8631. doi:10.1175/JCLI-D-16-0725.1.
Tsuruta, A., Aalto, T., Backman, L., Hakkarainen, J., van der Laan-Luijkx, I. T., Krol, M. C., et al. (2017). Global methane emission estimates for 2000–2012 from CarbonTracker Europe-CH₄ v1.0. *Geosci. Model Dev.* 10, 1261–1289. doi:10.5194/gmd-10-1261-2017.
Tucker, C. J., Pinzon, J. E., Brown, M. E., Slayback, D. A., Pak, E. W., Mahoney, R., et al. (2005). An extended AVHRR 8-km NDVI dataset compatible with MODIS and SPOT vegetation NDVI data. *Int. J. Remote Sens.* 26, 4485–4498. doi:10.1080/01431160500168686.
Turnbull, J. C., Mikaloff Fletcher, S. E., Ansell, I., Brailsford, G. W., Moss, R. C., Norris, M. W., et al. (2017). Sixty years of radiocarbon dioxide measurements at Wellington, New Zealand: 1954–2014. *Atmos. Chem. Phys.* 17, 14771–14784. doi:10.5194/acp-17-14771-2017.
van der Laan-Luijkx, I. T., van der Velde, I. R., van der Veen, E., Tsuruta, A., Stanislawska, K., Babenhauserheide, A., et al. (2017). The CarbonTracker Data Assimilation Shell (CTDAS) v1.0: implementation and global carbon balance 2001–2015. *Geosci. Model Dev.* 10, 2785–2800. doi:10.5194/gmd-10-2785-2017.
Vanselow-Algan, M., Schmidt, S. R., Greven, M., Fiencke, C., Kutzbach, L., and Pfeiffer, E.-M. (2015). High methane emissions dominated annual greenhouse gas balances 30 years after bog rewetting. *Biogeosciences* 12, 4361–4371. doi:10.5194/bg-12-4361-2015.
Verheijen, F. G. A., Zhuravel, A., Silva, F. C., Amaro, A., Ben-Hur, M., and Keizer, J. J. (2019). The influence of biochar particle size and concentration on bulk density and maximum water holding capacity of sandy vs sandy loam soil in a column experiment. *Geoderma* 347, 194–202. doi:10.1016/j.geoderma.2019.03.044.
Wakita, M., Nagano, A., Fujiki, T., and Watanabe, S. (2017). Slow acidification of the winter mixed layer in the subarctic western North Pacific. *J. Geophys. Res. Ocean.* 122, 6923–6935. doi:10.1002/2017JC013002.
Wang, F., Maksyutov, S., Tsuruta, A., Janardanan, R., Ito, A., Sasakawa, M., et al. (2019a). Methane Emission Estimates by the Global High-Resolution Inverse Model Using National Inventories. *Remote Sens.* 11, 2489. doi:10.3390/rs11212489.
Wang, S., Ma, S., Shan, J., Xia, Y., Lin, J., and Yan, X. (2019b). A 2-year study on the effect of biochar on methane and nitrous oxide emissions in an intensive rice–wheat cropping system. *Biochar* 1, 177–186. doi:10.1007/s42773-019-00011-8.
Wanninkhof, R. (1992). Relationship between wind speed and gas exchange over the ocean. *J. Geophys. Res.* 97, 7373. doi:10.1029/92JC00188.
Wanninkhof, R. (2014). Relationship between wind speed and gas exchange over the ocean revisited. *Limnol. Oceanogr. Methods* 12, 351–362. doi:10.4319/lom.2014.12.351.
Weiss, R. F. (1974). Carbon dioxide in water and seawater: the solubility of a non-ideal gas. *Mar. Chem.* 2, 203–215. doi:10.1016/0304-4203(74)90015-2.
Williams, N. L., Juranek, L. W., Feely, R. A., Johnson, K. S., Sarmiento, J. L., Talley, L. D., et al. (2017). Calculating surface ocean pCO2 from biogeochemical Argo floats equipped with pH: An uncertainty analysis. *Global Biogeochem. Cycles* 31, 591–604. doi:10.1002/2016GB005541.
Williamson, P., & Bodle, R. (2016). Update on climate geoengineering in relation to the convention on biological diversity: potential impacts and regulatory framework. Montreal.
Williamson, P., Wallace, D. W. R., Law, C. S., Boyd, P. W., Collos, Y., Croot, P., et al. (2012). Ocean fertilization for geoengineering: A review of effectiveness, environmental impacts and emerging governance. *Process Saf. Environ. Prot.* 90, 475–488. doi:10.1016/j.psep.2012.10.007.
Wilson, D., Blain, D., Couwenberg, J., Evans, C.D., Murdiyarso, D., Page, S.E., Renou-Wilson, F., Rieley, J.O., Sirin, A., Strack, M. & Tuittila, E.-S. (2016). Greenhouse gas emission factors associated with rewetting of organic soils. *Mires Peat* 17, 1–28. doi:10.19189/MaP.2016.OMB.222.
Wilson, D., Farrell, C. A., Fallon, D., Moser, G., Müller, C., and Renou-Wilson, F. (2016). Multiyear greenhouse gas balances at a rewetted temperate peatland. *Glob. Chang. Biol.* 22, 4080–4095. doi:10.1111/gcb.13325.
Wolter, K., and Timlin, M. S. (1998). Measuring the strength of ENSO events: How does 1997/98 rank? *Weather* 53, 315–

324. doi:10.1002/j.1477-8696.1998.tb06408.x.
Wolter, K., and Timlin, M. S. (2011). El Niño/Southern Oscillation behaviour since 1871 as diagnosed in an extended multivariate ENSO index (MEI.ext). *Int. J. Climatol.* 31, 1074–1087. doi:10.1002/joc.2336.
Woolf, D., Amonette, J. E., Street-Perrott, F. A., Lehmann, J., and Joseph, S. (2010). Sustainable biochar to mitigate global climate change. *Nat. Commun.* 1, 56. doi:10.1038/ncomms1053.
Worrall, F., Boothroyd, I. M., Gardner, R. L., Howden, N. J. K., Burt, T. P., Smith, R., et al. (2019). The Impact of Peatland Restoration on Local Climate: Restoration of a Cool Humid Island. *J. Geophys. Res. Biogeosciences* 124, 1696–1713. doi:https://doi.org/10.1029/2019JG005156.
Xue, L., Yu, W., Wang, H., Jiang, L.-Q., Feng, L., Gao, L., et al. (2014). Temporal changes in surface partial pressure of carbon dioxide and carbonate saturation state in the eastern equatorial Indian Ocean during the 1962–2012 period. *Biogeosciences* 11, 6293–6305. doi:10.5194/bg-11-6293-2014.
Yang, shihong, Xiao, Y., Sun, X., Ding, J., Jiang, Z., and Xu, J. (2019). Biochar improved rice yield and mitigated CH4 and N2O emissions from paddy field under controlled irrigation in the Taihu Lake Region of China. *Atmos. Environ.* 200, 69–77. doi:10.1016/j.atmosenv.2018.12.003.
Yin, Y., Chevallier, F., Ciais, P., Broquet, G., Fortems-Cheiney, A., Pison, I., et al. (2015). Decadal trends in global CO emissions as seen by MOPITT. *Atmos. Chem. Phys.* 15, 13433–13451. doi:10.5194/acp-15-13433-2015.
Yoshida, Y., Kikuchi, N., Morino, I., Uchino, O., Oshchepkov, S., Bril, A., et al. (2013). Improvement of the retrieval algorithm for GOSAT SWIR XCO2 and XCH4 and their validation using TCCON data. *Atmos. Meas. Tech.* 6, 1533–1547. doi:10.5194/amt-6-1533-2013.
Zeng, J., Nojiri, Y., Landschützer, P., Telszewski, M., and Nakaoka, S. (2014). A Global Surface Ocean f CO 2 Climatology Based on a Feed-Forward Neural Network. *J. Atmos. Ocean. Technol.* 31, 1838–1849. doi:10.1175/JTECH-D-13-00137.1.
Zhang, Y., Hu, X., Zou, J., Zhang, D., Chen, W., Liu, Y., et al. (2018a). Response of surface albedo and soil carbon dioxide fluxes to biochar amendment in farmland. *J. Soils Sediments* 18, 1590–1601. doi:10.1007/s11368-017-1889-8.
Zhang, Y., Joiner, J., Hamed Alemohammad, S., Zhou, S., and Gentine, P. (2018b). A global spatially contiguous solar-induced fluorescence (CSIF) dataset using neural networks. *Biogeosciences* 15. doi:10.5194/bg-15-5779-2018.
Zhou, M., Wang, X., Ke, Y., and Zhu, B. (2019). Effects of afforestation on soil nitrous oxide emissions in a subtropical montane agricultural landscape: A 3-year field experiment. *Agric. For. Meteorol.* 266–267, 221–230. doi:https://doi.org/10.1016/j.agrformet.2019.01.003.
Zickfeld, K., Azevedo, D., Mathesius, S., and Matthews, H. D. (2021). Asymmetry in the climate-carbon cycle response to positive and negative CO2 emissions. accepted.